Heliyon 9 (2023) e17282

Contents lists available at ScienceDirect

Heliyon

journal homepage: www.cell.com/heliyon

Studying the impacts of test condition and nonoptimal positioning of the sensors on the accuracy of the in-situ U-value measurement

Behnam Mobaraki [a,*], Francisco Javier Castilla Pascual [b], Arturo Martínez García [c,d], Miguel Ángel Mellado Mascaraque [e], Borja Frutos Vázquez [c], Carmen Alonso [c]

[a] Department of Civil and Building Engineering, Universidad de Castilla-La Mancha (UCLM), Av. Camilo Jose Cela s/n, 13071, Ciudad Real, Spain
[b] Department of Applied Mechanics and Project Engineering, Universidad de Castilla-La Mancha (UCLM), Escuela Técnica Superior de Ingenieros Industriales, 02071, Albacete, Spain
[c] Instituto de Ciencias de la Construcción Eduardo Torroja. Consejo Superior de Investigaciones Científicas (IETcc-CSIC), Serrano Galvache 4, 28033, Madrid, Spain
[d] Departamento de Construcción y Tecnología Arquitectónicas. Universidad Politécnica de Madrid (UPM), Escuela Técnica Superior de Arquitectura de Madrid, 28040. Av. Juan de Herrera 4, Madrid, Spain
[e] Department of Civil and Building Engineering, Universidad de Castilla-La Mancha (UCLM), Escuela Politécnica de Cuenca, Campus Universitario, 16071, Cuenca, Spain

ARTICLE INFO

Keywords:
Thermal transmittance parameter
Temperature-based method
Heat flux meter method
Building thermal monitoring
Energy efficiency
HEAT

ABSTRACT

The non-destructive thermal characterization of building envelopes relies significantly on various factors such as climate conditions, monitoring devices used, indoor environment, and conditioning systems. In the case of both the temperature-based method (TBM) and heat flux meter (HFM) approaches, U-value is determined considering the ideal condition of steady state. However, it is challenging to accurately define the true thermal condition of buildings when monitoring is affected by inherent uncertainties of the chosen approach and inadequate instrumentation of building envelopes. This paper presents the outcomes of an experimental campaign, that aimed to evaluate the impact of incorrectly positioned exterior sensors, on the precision of U-value measurements. This study simultaneously employed the TBM and HFM approaches. To enhance the accuracy of the results, rigorous outlier detection and statistical analysis were employed on the data collected from three autonomous monitoring systems. The findings of this study revealed that the applied data analysis yielded more satisfactory results for the TBM approach compared to HFM. However, regardless of the approach used, the effectiveness of outlier detection relied heavily on the accuracy of the monitoring systems. When removing an individual outlier, the monitoring systems characterized with higher accuracies provided U-values that were closer to the theoretical values, than less accurate ones.

1. Introduction

The U-value describes the rate of heat transfer through building envelopes in an optimal stationary condition. This parameter plays

* Corresponding author.
E-mail addresses: behnam.mobaraki@uclm.es (B. Mobaraki), fcojavier.castilla@uclm.es (F.J. Castilla Pascual), arturo.martinez@ietcc.csic.es, arturo.martinez.garcia@alumnos.upm.es (A.M. García), miguelangel.mellado@madrid.org (M.Á. Mellado Mascaraque), borjafv@ietcc.csic.es (B.F. Vázquez), c.alonso@ietcc.csic.es (C. Alonso).

https://doi.org/10.1016/j.heliyon.2023.e17282
Received 20 December 2022; Received in revised form 12 June 2023; Accepted 13 June 2023
Available online 14 June 2023

a crucial role in conducting effective energy audits for buildings [1]. The theoretical calculation of the U-value relies on a comprehensive understanding of the physical and mechanical characteristics of the building envelopes, including thickness, grain size, porosity, moisture content, and density [2]. However, in cases where this information is unavailable, non-destructive methods have been employed to estimate the U-value and assess the thermal performance of the building envelopes [3]. Destructive tests like endoscopy or coring, which provide the necessary mechanical properties of the building envelopes, are not always practical or feasible [4]. These methods, though effective, are not commonly used in routine restoration practices due to their high cost in terms of time, money, and the need for specialized technical expertise. In such situations, the estimation of the U-value can only be performed in-situ, where the composition of the envelopes is unknown. Consequently, comparing theoretical results with experimental data becomes a challenging task.

In fact, the accuracy of in-situ U-value calculation through monitoring is greatly influenced by the chosen approach. In the existing literature [5], experts commonly utilize two widely employed approaches: Heat Flux Meter (HFM) [6] and Temperature-Based Method (TBM) [7]. HFM is a non-destructive method used for thermal characterization of building envelopes. It follows the guidelines outlined in the ISO 9869-1:2014 standard [8]. This approach calculates the U-value of building envelopes by dividing the heat flux rate by the temperature difference between indoor and outdoor, under steady state monitoring conditions [8]. Due to the variation of meteorological parameters, it is difficult to achieve the steady state condition in the field [9]. To overcome this challenge [8], suggests an alternative solution, which involves assuming the average values of heat flux and temperatures over the monitoring period (a minimum of three days) as an estimation of the steady state conditions. However, to ensure reliable measurement results, scholars commonly recommend a monitoring period of approximately two weeks [10]. The TBM approach follows Newton's law of cooling for the measurement of U-value. According to this law, the heat transfer rate is proportional to the temperature difference between the object and its surroundings [11]. Instead of direct measurement of the heat flux, the TBM approach determines the U-value by measuring the heat transfer coefficient of the building envelopes (h_{in}) and three temperature parameters which are interior (T_i), exterior (T_e), and interior surface temperature of the wall (T_{si}).

The standard conditions for measuring h_{in} involve an exterior temperature of 10 °C, an interior temperature of 20 °C, and an exterior wind speed of 4 m/s [12]. However, achieving these conditions in the field can be challenging due to the fluctuations in exterior temperature and speed of the wind. To overcome this challenge, some of the commercial solutions consider the value of h_{in} based on the information provided in the ISO 6946:2021-12-29 standard [12]. Schematics of the TBM and HFM approaches are presented in Fig. 1(a) and (b), respectively. These figures also presented the required parameters for the U-value calculation. In these figures, q represents the heat flux, while the other temperature parameters have been explained in the previous paragraph.

The TBM approach offers a significant advantage over the HFM approach by eliminating the need for a costly heat flux sensor, which can introduce inaccuracies in U-value measurements [13]. By employing effective data processing techniques and a suitable monitoring strategy, the uncertainties arising from inappropriate environmental conditions can be greatly mitigated. One approach to address temperature fluctuations and reduce monitoring errors is to increase the temperature difference (ΔT) between the interior and exterior of the building. Previous studies in the literature suggests various ranges of ΔT for precise building characterization [14,15]. However, determining the specific ΔT for accurate calculation of the U-value is challenging as it depends on numerous factors. A referenced study [16] demonstrated the effectiveness of a novel data analysis methodology, resulting in a reduction of the difference between measured and calculated U-values from 36.9% to −7.6%. Feuermann proposed a methodology for estimation of U-values in different buildings by employing a steady-state heat balance and averaging data over several days [17]. In Ref. [18], the authors considered the wind velocity when analyzing both surface heat flux and temperature samples.

Different solutions have been proposed in the literature to increase the accuracy of building thermal monitoring [13]. Rasooli and

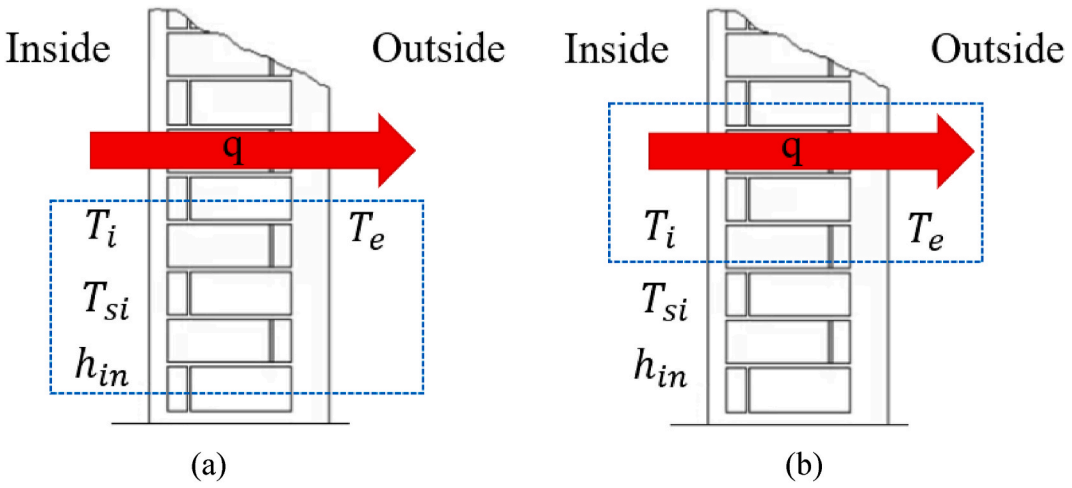

Fig. 1. The schematic of TBM and HFM approaches and the parameters to be considered for calculation of the U-value. (a) TBM: T_i, T_e, T_{si}, and h_{in}. (b) HFM: T_i, T_e, and q.

Itard proposed the installation of an additional heat flux sensor on the opposite side of the wall [10]. Evangelisti et al. conducted a comprehensive analysis of the fundamental principles underlying both the HFM and TBM approaches [19]. They specifically investigated the influence of the vertical profile of indoor air temperature. The results revealed that the deviation percentage between experimental results (using the HFM approach) and the theoretical values exceeded 20%, when the indoor temperature sensors were positioned at 1.8 m or higher. Desogus et al. compared the HFM approach with destructive methods to assess the uncertainties in humid Mediterranean climate conditions [20]. The authors concluded that the HFM approach provides the most accurate R-value, when the favorable environmental conditions are available ($\Delta T = 10\ ^{\circ}C$). However, in cases where these conditions are not met, both methods can be applied with less precision. In another study [21], the authors proposed a novel methodology to enhance the accuracy of building characterization by increasing the number of measurements and applying statistical analysis to the monitoring data.

A thorough analysis of the TBM and HFM approaches was carried out by reviewing the past research presented research papers from 2013 to 2022. The findings of this evaluation are presented in Table 1, which provides a summary of the test period, verification method, deviation, source of uncertainty, publication year and the associated reference in the literature. The table also highlights deviation between the results obtained from both the TBM and HFM approaches and the reference values. Furthermore, the source of uncertainty refers to limitation of the monitoring performed are presented.

ISO 9869-1:2014 states that if ideal monitoring conditions are achieved, the overall monitoring error is expected to fall within the range of 14%–28%. However, previous research [26] has reported higher levels of error. The accurate building thermal monitoring relies on various factors such as climate conditions, layout, homogeneity, moisture content, and instrumentation [26]. Previous studies indicated that the uncertainty in building characterization can reach up to 37% due to the orientation of the envelopes [34]. To minimize the impact of direct solar radiation (S.R), it is recommended to instrument and monitor walls facing north and south [35]. It has been demonstrated that selecting walls facing south for monitoring can reduce the uncertainty to 10% [36,37]. Additionally, when measuring surface temperature, it is important to consider the effects of thermal boundary conditions, wind speed, and snow [38,39]. This highlights the need for the monitoring point to be representative of the entire envelope.

Other researchers have focused on reducing the uncertainty in U-value measurements related to instrumentation of building envelopes [13]. Meng et al. conducted a study on the uncertainties associated with the positioning of thermocouples and heat flux sensors, as well as the size, shape, and angle of attachment of heat flux sensors, when using the HFM approach to measure U-value [23]. The authors emphasized that proper sensor installation greatly enhances monitoring accuracy. They found that the uncertainty could reach up to 6% when thermocouples are not correctly attached, and up to 26% when heat flux sensors are not properly positioned. It is also crucial to appropriately position indoor sensors to mitigate the influence of heat sources. In other words, when a heating system is activated or solar radiation enters through openings or windows, convective and radiative thermal energy affects the heat flux sensor. Consequently, the measured heat flow increases, leading to an artificially higher calculated U-value, which does not accurately represent the actual thermal condition of the envelopes. Furthermore, sensor placement should avoid thermal bridges near windows, corners, floors, and ceilings [40].

The use of infrared thermography (IRT) has been widespread in monitoring the thermal conditions of buildings [1]. This method can also be applied to support the positioning of sensors in TBM and HFM approaches by qualitatively analyzing the building envelopes. It helps identify issues [41], detachment [42], and thermal anomalies. Lucchi conducted an in situ study, examining various historic brick masonry structures with various historical ages and intended uses [43]. In this study, IRT was utilized to assess the thermal homogeneity, presence of cracks, and moisture content. The author then compared the collected data with standards to evaluate the thermo-physical behavior of old walls, providing guidance for energy audits of monuments. Lucchi et al. also introduced a test procedure that employed a hot box apparatus to study the thermal performance of a masonry wall [44]. To accomplish this, IRT

Table 1
Summary of the reviewed articles associated with thermal monitoring of buildings using HFM and TBM approaches (2013–2022).

Approach	Test period (Day)	verification method	Deviation (%)	Source of uncertainty	Year	Ref.
HFM	4	Theoretical method	20.00–46.00%	Sensitivity to dynamic conditions, input data, initial thermal field inside the element for the post-processing method	2013	[22]
	7	Theoretical method	14.00–28.00%	Measurement instrumentation and weather condition	2014	[6]
	Numerical study	Thermoelectricity analogy theory	6.00–26.00%	Improper pasting of sensor	2015	[23]
	3	Thermal imaging survey	3.92–10.77%	Moisture content, workmanship, and accuracy of measuring equipment	2015	[24]
	8	Theoretical method	12.45–21.84%	Low- temperature difference between inside and outside	2015	[25]
	3 to 7	Theoretical method	8.00–50.00%	Ambient condition	2015	[26]
	3	Theoretical method	1.00–5.00%	Weather condition	2016	[27]
	3 to 30	Theoretical method	6.00–18.00%	Direction of heat flow	2017	[28]
	7	Theoretical method	1.90–7.30%	Temperature difference between inside and outside	2018	[29]
	7 to 18	Theoretical method	20.12%–60.96%	Thermal boundary conditions	2020	[30]
TBM						
	4	HFM	2.00%	Malfunctioning of the used sensors	2017	[31]
	3	Theoretical method	6.00–13.00%	Weather condition	2018	[14]
	7	Theoretical calculation	1.00–7.00%	Uncertainty of the device	2019	[32]
	7	Theoretical calculation (ISO6946)	75.00–90.00%	Achieving stability in measurements with high thermal gradient	2019	[33]

was adopted to measure the thermal characteristics of the wall surface at various levels and to obtain more accurate plans for the installation of temperature and heat flux sensors. Through the IRT survey, the authors investigated several factors: (1) Surface irregularities in terms of thermal patterns. (2) Identification of thermal bridges and their corresponding thermally influenced areas. (3) Assessment of the distribution of aerogel insulation. (4) Qualitative assessment of surface moisture levels. In Ref. [45], the authors developed an on-site hot box apparatus to assess the hygrothermal performance of historic masonry buildings. It was observed that the size, shape, and location of the region of interest (ROI) significantly impact the interpretation of U-value estimations due to the presence of thermal bridges and irregularities. Mahmoodzadeh et al. demonstrated that U-value measurements using IRT, in the best-case scenario depends on the ROI location, U-value deviated from nominal U-values by 6.25%–25% [46].

In order to improve the accuracy of building monitoring using TBM and HFM approaches, it is important to consider the impact of outliers originating from different sources during the monitoring. To address this issue, IoT solutions can be employed to facilitate data filtration [47]. In this context, several IoT-based architectures have been proposed in the literature with various objectives, such as enhancing the reliability and efficiency of data collection processes [48], analyzing indoor thermal comfort [49], evaluating energy savings in buildings [50], studying the influence of transient facades on indoor air quality [51], and enabling real-time monitoring of energy consumption [52]. Furthermore, to overcome the high costs associated with commercial monitoring systems [53], several low-cost methodologies have been suggested. These solutions aim to monitor air quality [54], monitor the interior temperature [55], provide energy usage data [56], conduct destructive thermal monitoring of buildings [31], obtain the thermal parameters of building envelopes [57], measure the level of humidity [58], and monitor other interior and exterior parameters of buildings [59]. As a result, the integration of low-cost sensors and IoT has been investigated to improve the characterization of the U-value [60].

According to existing literature, performing in-situ building characterization becomes challenging when TBM and HFM approaches are employed to determine the U-value. The accurate measurement of in-situ U-values requires the appropriate instrumentation of building envelopes, which involves locating exterior sensors opposite to interior sensors. Nevertheless, the layout of the building envelopes or administrative constraints may prevent engineers from installing outdoor sensors at the ideal location. In such situations, a possible strategy is to place the exterior sensors at the nearest windowsill or jam, although this approach does not align with ISO 9869-1:2014 guidelines. Literature currently lacks sufficient research on quantifying the level of uncertainty arising from this situation and exploring methods to accurately characterize U-values.

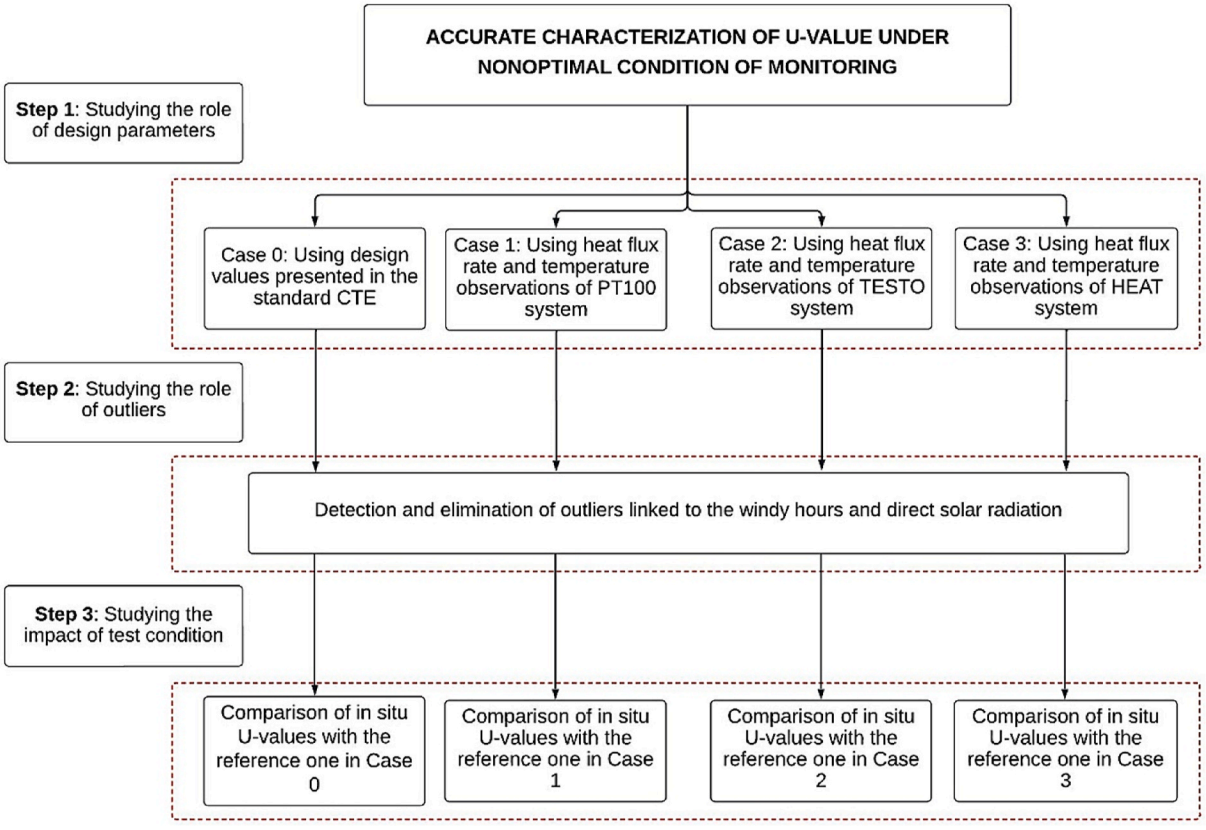

Fig. 2. Research methodology.

2. Aim and methodology

The originality of this study is to accurately determine the U-value of building envelopes, even in cases where the location of exterior sensors does not meet the optimal conditions specified by standards. Therefore, the scope of this study revolves around three important factors that need to be investigated: (1) The influence of design parameters necessary for estimating theoretical and in-situ U-values, such as the internal heat transfer coefficient (h_{in}), internal surface resistance of the wall (R_{si}), and external surface resistance of the wall (R_{se}), (2) the impact of outliers, and (3) the significance of test conditions. To accomplish this, the research methodology is as follows:

Step 1 The influence of design parameters. In this step, the design parameters required for calculation of the theoretical and experimental U-values were considered from different available sources. The data sources utilized included the Spanish building standard (Código Técnico de la Edificación, CTE) [61], as well as the results from three distinct monitoring systems. These systems consisted of the author's novel IoT Hyper Efficient Arduino Transmittance-meter (IoT HEAT), along with two commercially available solutions, namely the TESTO 635-2 and PT100. Based on this, the study defined four different cases for analysis, as follows:

- Case 0 Employing the design parameter values specified in CTE [61].
- Case 1 Utilizing the heat flux rate measured by the heat flux sensor, along with the temperature data obtained from the PT100 system, enabling the calculation of design parameters.
- Case 2 Utilizing the heat flux rate measured by the heat flux sensor, along with the temperature data obtained from the TESTO 635-2 system, enabling the calculation of design parameters.
- Case 3 Utilizing the heat flux rate measured by the heat flux sensor, along with the temperature data obtained from the IoT HEAT system, enabling the calculation of design parameters.

Step 2 The impact of outliers associated with meteorological factors. Thorough data analysis was employed to study the monitoring data logged from an individual monitoring system. In this step, all the outliers caused by windy hour (W·H) and direct solar radiation on sensors were removed.

Step 3 The in-situ U-values were calculated considering the temperature parameters captured by each monitoring system and the h_{in} of the associated case (when studying the TBM approach). In the end, the obtained in-situ U-values achieved from the monitoring systems were compared to the reference U-value of the respective case. This comparison aimed to determine a representative U-value for the case study. Fig. 2 provides a concise overview of the steps undertaken for the U-value characterization.

In order to assess the reliability of the data analysis in this study, an uncertainty analysis was conducted. Following the recommendations of [7,62], the standard deviation analysis was employed to evaluate the monitoring data at various stages of the $\Delta T \geq X°C$ pattern. Regarding the IoT HEAT, this system underwent verification in a controlled condition of laboratory [63], as well as in unsteady state condition of monitoring, to characterize an educational building in Spain [64]. The principal novelties of IoT HEAT are as follows: (1) The monitoring system functions by utilizing affordable medical sensors that don't require physical contact to measure the temperature of building surfaces. This new development eliminates the inaccuracies present in contact sensors used for building

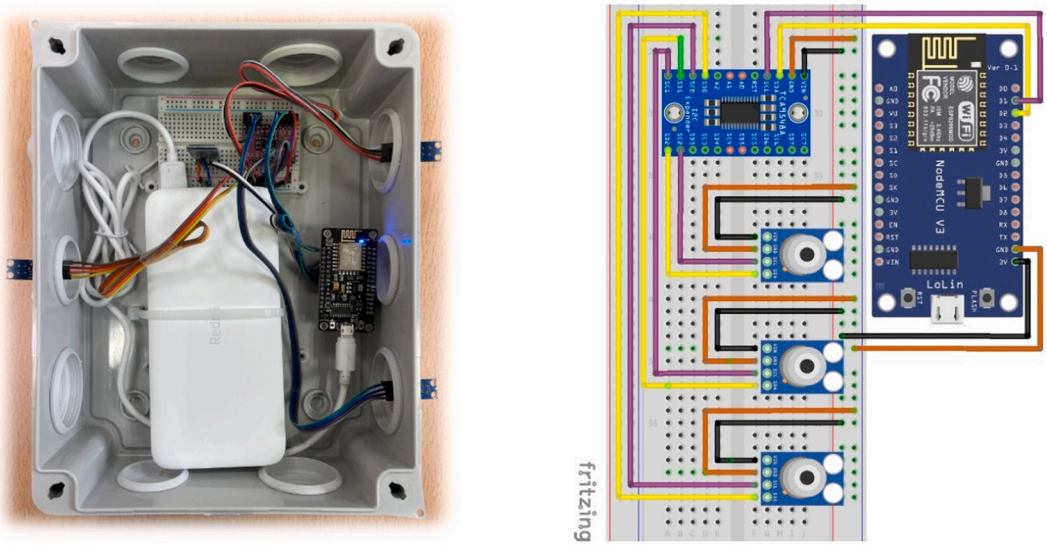

Fig. 3. HEAT indoor module (a), and the associated wiring connection (b).

analysis, which were reported to have an error rate of up to 5% [14]. (2) Differing from conventional commercial solutions, this monitoring system functions using an inexpensive wireless communication protocol such as Bluetooth and the Internet. This innovative approach eliminates the potential risk of data loss while conducting monitoring. (3) The integration of cloud computing into IoT HEAT facilitated real-time monitoring of buildings and enabled the postprocessing of monitoring data. As a result, during this monitoring campaign, the chosen building envelope was continuously monitored in real-time, and the gathered measurements were promptly filtered and postprocessed in real-time as well.

3. Monitoring systems

This section outlines the features of the used monitoring systems in relation to their components and levels of accuracy.

3.1. HEAT

HEAT was created using the NodeMCU ESP8266 and cheap sensors. In HEAT, the calculation of U-value is performed using the TBM method. The HEAT outdoor module was equipped with eight units of SHT35 sensors that conducted synchronized measurements of the outdoor temperature [65]. The sensor utilized in this system has the capacity to detect temperatures ranging from −40 to +125 °C, with a precision of 0.2 °C. In the indoor module, three MLX90614 sensors were employed, which are contactless and capable of measuring the ambient temperature as well as the surface temperature of an object simultaneously [66]. With an accuracy of ±0.5 °C, this sensor offers a detection range of −40 to +125 °C for ambient temperature and −70 to +380 °C for object temperature. Each HEAT module is equipped with a 20,000 mAh Power bank, ensuring sufficient power supply for monitoring purposes. Furthermore, the TCA9548A multiplexer was employed to increase the data transmission capacity of the sensor network developed, enabling the multiplexing of sensors. Fig. 3(a) and (b) display the HEAT indoor module and its corresponding wiring diagram generated using Fritzing software. Similarly, Fig. 4(a) and (b) depict the outdoor module of HEAT along with its associated wiring diagram.

From the various IoT platforms available, ThingSpeak was selected to visualize, aggregate, and process real-time measurements. This platform, in collaboration with MathWorks, allows users to perform calculations on the data and construct data models using any function within the MatLab toolboxes. Regarding their operation, the HEAT modules transmit measurements to the ThingSpeak platform according to the specified sampling frequency programmed in the microcontroller algorithm. This means that each HEAT module functions independently, and the U-value calculation of the analyzed building envelope is carried out using a designated script within the IoT platform. The calculation occurs when the data is received in a designated field within the assigned channel of the platform.

3.2. TESTO 635-2

To determine the U-value using the TESTO 635-2, the following equipment (as shown in Fig. 5) was utilized. (1), the Testo 635-2:

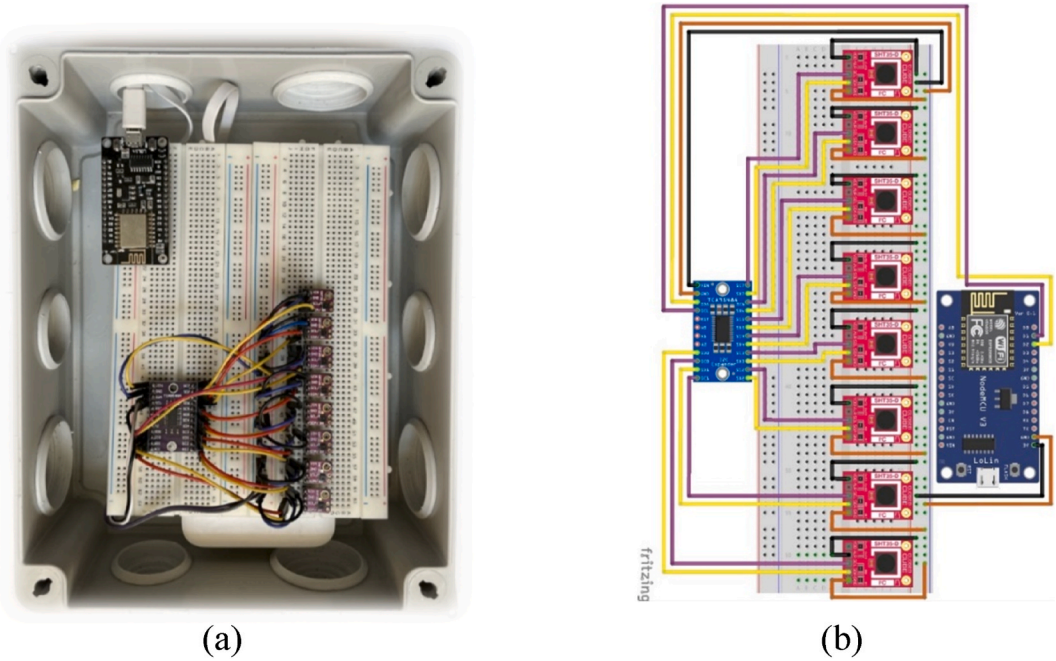

Fig. 4. HEAT outdoor module (a), and the associated wiring connection (b).

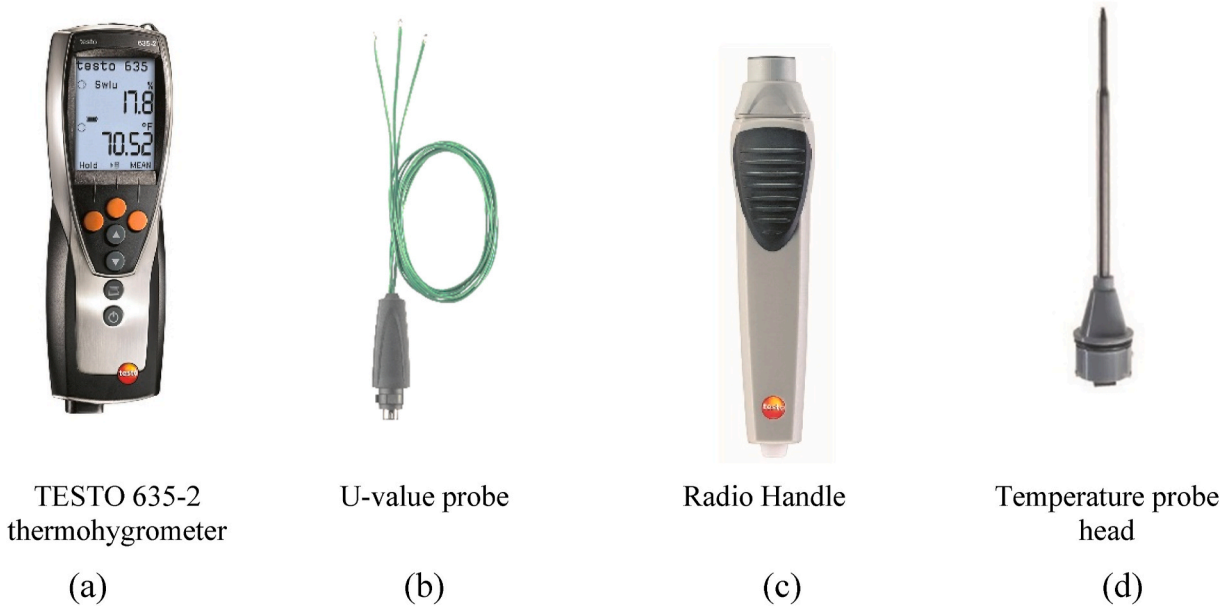

Fig. 5. Instrumentation used for installation of TESTO 635-2 monitoring system: TESTO 635-2 thermohygrometer (a), U-value probe (b), Radio handle (c), and temperature probe head (d).

This data logger (depicted in Fig. 5(a)) was employed, which has a memory capacity capable of storing approximately 10,000 readings. The captured parameters can be accessed and downloaded using the Comfort Software provided by the same company. TESTO 635-2 calculates the U-value using the TBM method by measuring the indoor and outdoor temperatures, as well as the indoor surface temperature of the building envelopes. The device allows for adjustments to introduce the total internal heat transfer coefficient. (2) Internal surface temperature probe (depicted in Fig. 5(b)): In this study, a K-type probe (NiCr–Ni) was connected to the TESTO 635-2 device. The probe has an accuracy of ±0.3 °C within a temperature range of −200 °C to +1370 °C. To calculate the U-value, the probe incorporates three surface temperature thermocouples and one ambient temperature thermocouple into its connector. (3) Outdoor sensor: for measuring the outdoor air temperature a type K thermocouple with an accuracy of ± (0.5 °C + 0.3% of measured value) within a temperature range of −40 °C to +500 °C was employed (depicted in Fig. 5(c) and (d)). The module consists of a head and handle that establish a wireless connection to transmit its readings to the TESTO 635-2 device, providing the calculation of the U-value.

3.3. PT100

The monitoring system PT100 contains the following elements: (1) Resistance temperature detector: Pico PT100 1/10DIN type, which has the accuracy of ±0.04 °C. This system contains three sensors for the measurement of indoor, outdoor, and indoor surface temperatures of buildings (Fig. 6(a)). (2) Heat Flux Meter: Hukseflux HFP01 (Fig. 6(b)), which has the measurement range from −2000

Fig. 6. RTD probes with the associated data logger (a), and heat flux sensor with the associated data logger (b).

to +2000 W/m^2. This heat flux sensor comes with a Hukseflux LI-19 data logger which has the capacity to record 3518 measurements. The information is stored in the data logger and must be downloaded to a computer before it reaches its maximum capacity.

4. Case study description

The monitored wall is situated in an unoccupied apartment within a residential building in Madrid, Spain. The building, constructed in 1968, is situated in a densely populated urban area with medium-height structures consisting of 6–7 floors. The monitoring period took place over four days during winter (February 2022), with measurements being recorded at a sampling frequency of 15 min. It is important to note that the heating system in the apartment was turned off throughout the monitoring period. The building's walls face northeast, southeast, and east, and for the study, the northeast-facing wall was chosen to install inner sensors away from windows, thus avoiding thermal bridges. This particular section of the wall receives direct sunlight for approximately 2 h per day during the experiment. It is recommended to conduct U-value measurements on a north-facing façade to eliminate the impact of S.R, but this is often challenging in urban areas like this one. Fig. 7(a) and (b) depict the monitored wall and the geographical orientation of the building, respectively.

The positioning of interior sensors followed the guidelines outlined in the ISO 9869-1:2014 standard, taking into consideration specific heights and distances from the walls. However, due to the apartment being situated on the fourth floor, installation of the outdoor modules posed a challenge. Ultimately, they were placed on the windowsill and jamb. However, it is important to note that this positioning deviates from the specifications outlined in the ISO 9869-1:2014. Fig. 8(a) provides a visual representation of the installation of the indoor modules from three monitoring systems on the northeast wall, while Fig. 8(b) illustrates the locations of the outdoor modules.

Regarding the TESTO 635-2 and PT100 devices, it is important to mention that the calculation of the U-value had to be performed after the monitoring campaign. In contrast, the HEAT system allowed for real-time monitoring of the U-value, as shown in Fig. 9.

5. Results

This chapter introduces the calculation of the theoretical U-value considering CTE standard. Subsequently, the results obtained from the experimental campaign using both the TBM and HFM approaches are presented for the three monitoring systems. As mentioned earlier, four sources of data were utilized to calculate the theoretical U-value. This parameter, "theoretical U-value", is here called the "reference U-value" ($U-value_{Ref}$).

5.1. Determination of the reference U-value based on CTE

The thermal conductivities of the various layers in the analyzed wall were determined using the CTE standard. Fig. 10 illustrates the composition of the wall, which comprises a 26 cm-thick uninsulated cavity wall. This cavity wall consists of a 12 cm layer of perforated

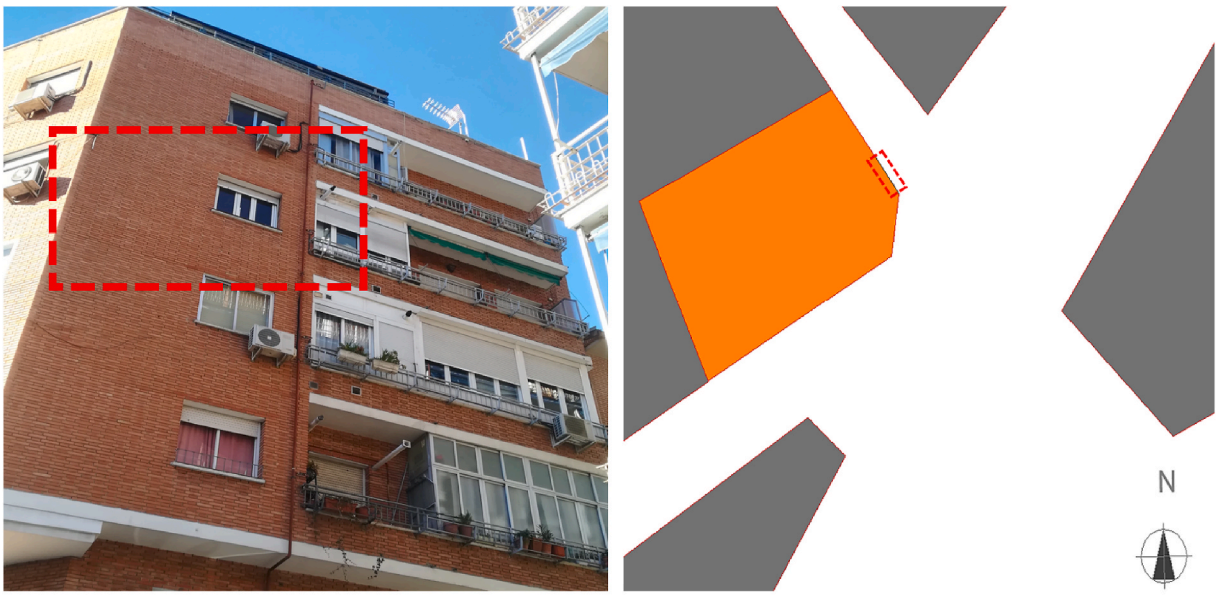

Fig. 7. Location of the studied envelope (a), geographical orientation of the building (b).

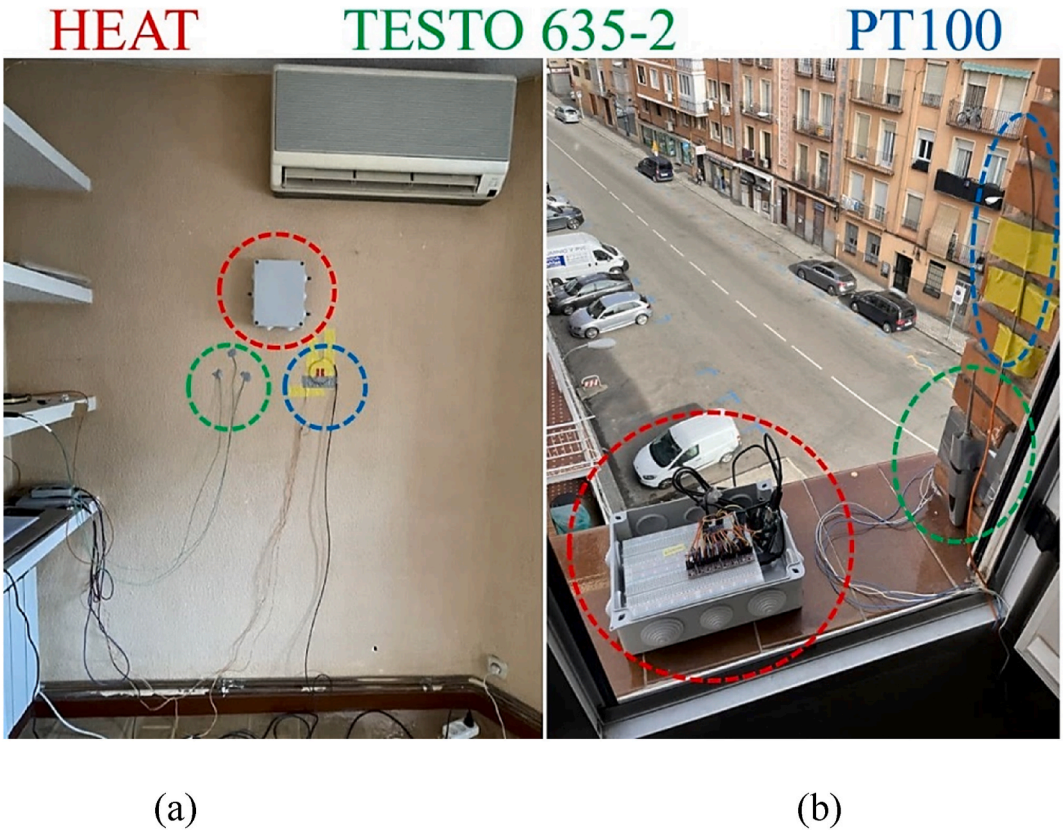

Fig. 8. Indoor modules of the three monitoring systems installed on the northeast wall (a), outdoor modules placed on the windowsill and jamb (b).

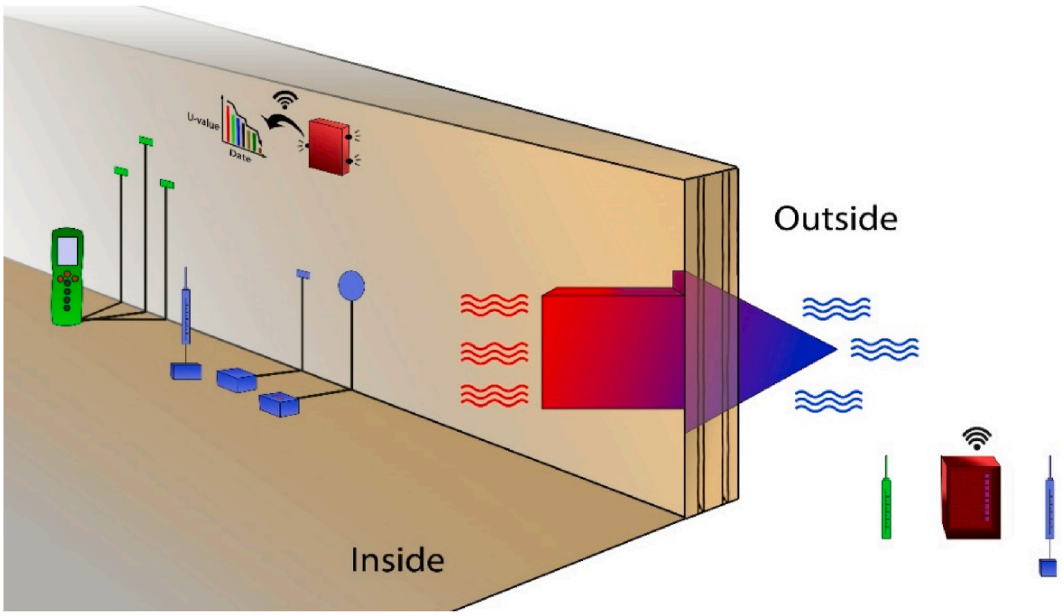

Fig. 9. Layout of the studied envelope showing the placement of sensors and the online (HEAT) and offline (TESTO and PT100) calculation of the U-value.

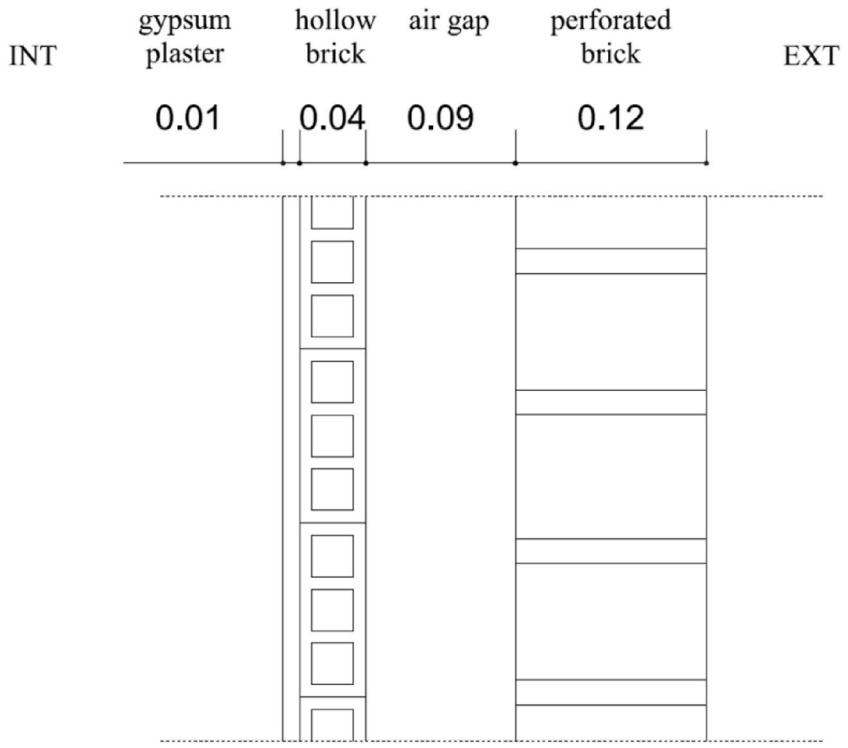

Fig. 10. Composition of the studied envelope.

Table 2
Composition of the wall and thermal characteristics of the different layers [a].

Composition	λ (W/m.K)	d (m)	R (m^2.K/W)
Perforated brick	0.350	0.120	0.343
Air gap (unventilated)	–	0.090	0.170
Hollow brick	0.320	0.040	0.125
Gypsum plaster	0.300	0.010	0.033
Total		0.260	0.671

[a] Some of the R-values for different layers were directly specified in the CTE, but others were calculated using the thermal conductivity, λ, and the thickness, d.

brick, followed by a 9 cm air gap and a 4 cm layer of hollow brick. The wall is finished with a 1 cm layer of gypsum plaster. Based on the obtained stratigraphy and the corresponding thermal parameters derived from the CTE standard, Table 2 is provided, outlining the thermal characteristics of the wall composition [61].

The $U-value_{Ref.}$ of the examined wall was determined by considering four different cases. These cases involved calculating the $U-value_{Ref.}$ based on the thermal resistances (R_{si} and R_{se}) derived from the following sources: the CTE standard (case 0), measurements obtained from the PT100 (case 1), measurements obtained from the TESTO 635-2 (case 2), and measurements obtained from the HEAT (case 3). For each specific case, the calculation of R_{si} and R_{se} was performed based on the temperature parameters obtained from the monitoring systems as follows [4]:

1. Obtain R_{si} from Eq. (1). This parameter is the inverse of the h_{in}.

$$R_{si}=\frac{\sum_{j=1}^{n}\left(T_{i(j)}-T_{si(j)}\right)}{\sum_{j=1}^{n}q_{(j)}} \tag{1}$$

2. Obtain the total value of surface thermal resistances (R_{st}) from Eq. (2):

$$R_t=R_{st}+\overline{R} \tag{2}$$

where, R_t is the total thermal resistance (inverse of the U-value) $\overline{R}$ is the thermal resistance, (inverse of the thermal conductance). $\overline{R}$ is calculated using Eq. (3):

$$\overline{R} = \frac{\sum_{j=1}^{n}\left(T_{si(j)} - T_{se(j)}\right)}{\sum_{j=1}^{n} q_{(j)}} \quad (3)$$

3. Obtain R_{se} from Eq. (4):

$$R_{st} = R_{si} + R_{se} \quad (4)$$

Table 3 displays the four designated scenarios along with the calculated parameters, including R_{si}, R_{se}, h_{in}, and the $U - value_{Ref.}$. The heat transfer coefficient must be determined under standard building monitoring conditions, with the exterior temperature set at 10 °C, the interior temperature at 20 °C, and an exterior wind speed of 4 m/s [12]. Nevertheless, during this monitoring campaign, it was not possible to meet the aforementioned conditions due to a limitation. This limitation can be attributed to the significant fluctuations in wind velocity and outdoor temperature between night and day, which are common in the dry continental Mediterranean region of Spain. Due to this limitation, it was recommended in the literature to determine the value of h_{in} based on the information provided in the CTE for R_{si} [14]. Similarly, in this study, taking into account the horizontal heat flow, the value of h_{in} for the wall was defined as 7.69 W/m^2.K [61]. This assumption was labeled as Case 0 in the study, as indicated in Table 3. According to the data provided in the table, the calculated value of R_{si} obtained from the measurements of PT100, TESTO, and HEAT is 46%, 61%, and 85% higher, respectively, compared to the value proposed by the CTE. In terms of R_{se}, the calculated value obtained from PT100 aligns with the value suggested by the CTE. However, the values derived from TESTO and HEAT are 50% lower and 250% higher, respectively, compared to the value specified in the CTE. These differences vividly illustrate the influence of sensor accuracy, with the PT100 system exhibiting the highest accuracy and yielding results that are closest to the design values defined in the CTE.

Moreover, due to the fluctuations in exterior temperature and wind, there was a higher level of uncertainty in estimating R_{se}, with variations of up to 250%, compared to R_{si}, which experienced variations of up to 85%. Lastly, taking into account the wall characteristics presented in Table 3, the $U - value_{Ref.}$ of 1.19 W/m^2.K, 1.10 W/m^2.K, 1.10 W/m^2.K, and 0.95 W/m^2.K were attained from the four respective cases (Table 3).

5.2. Results of the in-situ measurements

This subsection presents the results of U-value measurements obtained through both the TBM and HFM approaches. To analyze the monitoring data using the HFM approach, the measurements from heat flux sensors were combined with the necessary temperature parameters recorded from an individual system. This means that the data regarding interior and exterior temperatures, along with the heat flux rate at various time intervals, were utilized to estimate the U-value based on the HFM approach. In terms of thermal monitoring results using the TBM method with the TESTO system, it is important to note that the calculation of the in-situ U-value was performed manually. This involved extracting the monitored temperature parameters from the TESTO device and conducting post-processing of the data while considering the associated h_{in}. For Case 2, as shown in Table 3, the heat transfer coefficient considered for the TESTO system was 4.76 W/m^2.K. Similarly, the heat transfer coefficient was calculated and considered for the PT100 system (5.26 W/m^2.K) and the TESTO system (4.76 W/m^2.K).

5.2.1. Case 0

Table 4 displays the average U-values and uncertainty analysis of measurements for Case 0 at various stages, considering ΔT ranging from $\Delta T > 0$°C to $\Delta T \geq 12$°C. According to the results presented in Table 4, the maximum ΔT detected by the HEAT system is approximately 1 °C higher compared to the TESTO and PT100 systems. According to the information presented in the table, the average U-values obtained at different stages of the ΔT measured by the three monitoring systems are not consistent, both in the TBM and HFM conditions. This variation can be attributed to the inherent uncertainties associated with both methods and the varying accuracies of the sensors integrated into the monitoring systems. However, when comparing the temperature differences between day (*e.g.*, $\Delta T \geq 1$°C) and night (*e.g.*, $\Delta T \geq 8$), it can be concluded that the variation in U-values, as measured by three different monitoring systems, significantly decreases. Specifically, for the TBM analysis, the difference decreases from 0.35 W/m^2.K (2.13–1.78) to 0.07 W/m^2.K (1.30–1.23). A similar analysis of the monitoring periods for the HFM case shows a nearly identical reduction in difference, from 0.23 W/m^2.K (1.39–1.16) to 0.08 W/m^2.K (0.75–0.67).

Figs. 11, 12, and 13 display the obtained reference $U - value_{Ref.}$ in case 0, along with the time series graphs illustrating the measured T_i, T_e, T_{si}, $U - value_{TBM}$, and $U - value_{HFM}$ of the monitored wall. These measurements were derived from the HEAT, TESTO

Table 3
Calculation of internal and external surface resistances parameters and heat transfer coefficient according to the information presented in the CTE and the measurements of the three monitoring systems.

Case	Source of data	Design parameters			
		R_{si} (m^2.K/W)	R_{se} (m^2.K/W)	h_{in} (W/m^2.K)	*Ref. U-value* (W/m^2.K)
0	CTE	0.13	0.04	7.69	1.19
1	PT100	0.19	0.04	5.26	1.10
2	TESTO	0.21	0.02	4.76	1.10
3	HEAT	0.24	0.14	4.17	0.95

Table 4
Results of the U-values through TBM and HFM approaches for case 0.

ΔT (°C)	Average U-value (W/m².K)					
	Case 0					
	TBM			HFM		
	HEAT	PT100	TESTO	HEAT	PT100	TESTO
$\Delta T > 0$	2.13 ± 1.38	2.00 ± 1.56	2.28 ± 2.00	1.16 ± 0.89	1.51 ± 1.58	1.58 ± 1.79
$\Delta T \geq 1$	2.13 ± 1.37	1.78 ± 1.12	2.04 ± 1.54	1.16 ± 0.89	1.31 ± 1.22	1.39 ± 1.46
$\Delta T \geq 2$	2.05 ± 1.26	1.51 ± 0.56	1.66 ± 0.71	1.11 ± 0.85	1.03 ±0.73	1.04 ± 0.79
$\Delta T \geq 3$	1.76 ± 0.85	1.46 ± 0.45	1.57 ± 0.51	0.96 ± 0.66	0.97 ± 0.61	0.95 ± 0.59
$\Delta T \geq 4$	1.62 ± 0.65	1.39 ± 0.33	1.50 ± 0.40	0.87 ± 0.55	0.88 ± 0.48	0.88 ± 0.48
$\Delta T \geq 5$	1.46 ± 0.45	1.34 ± 0.27	1.45 ± 0.34	0.75 ± 0.41	0.82 ± 0.40	0.82 ± 0.41
$\Delta T \geq 6$	1.33 ± 0.22	1.30 ± 0.21	1.38 ± 0.23	0.67 ± 0.23	0.77 ± 0.30	0.75 ± 0.27
$\Delta T \geq 7$	1.28 ± 0.14	1.27 ± 0.18	1.35 ± 0.17	0.65 ± 0.17	0.73 ± 0.19	0.73 ± 0.20
$\Delta T \geq 8$	1.26 ± 0.12	1.23 ± 0.18	1.30 ± 0.13	0.67 ± 0.14	0.75 ± 0.16	0.73 ± 0.13
$\Delta T \geq 9$	**1.27 ± 0.11**	**1.20 ± 0.18**	**1.26 ± 0.12**	0.70 ± 0.10	0.73 ± 0.10	0.72 ± 0.10
$\Delta T \geq 10$	1.25 ± 0.06	1.03 ± 0.03	1.17 ± 0.07	0.70 ± 0.06	0.82 ± 0.05	0.78 ± 0.06
$\Delta T \geq 11$	1.22 ± 0.04	1.05 ± 0.01	1.19 ± 0.05	0.73 ± 0.04	0.86 ± 0.01	0.83 ± 0.03
$\Delta T \geq 12$	1.25 ± 0.03	–	–	0.77 ± 0.02	–	–

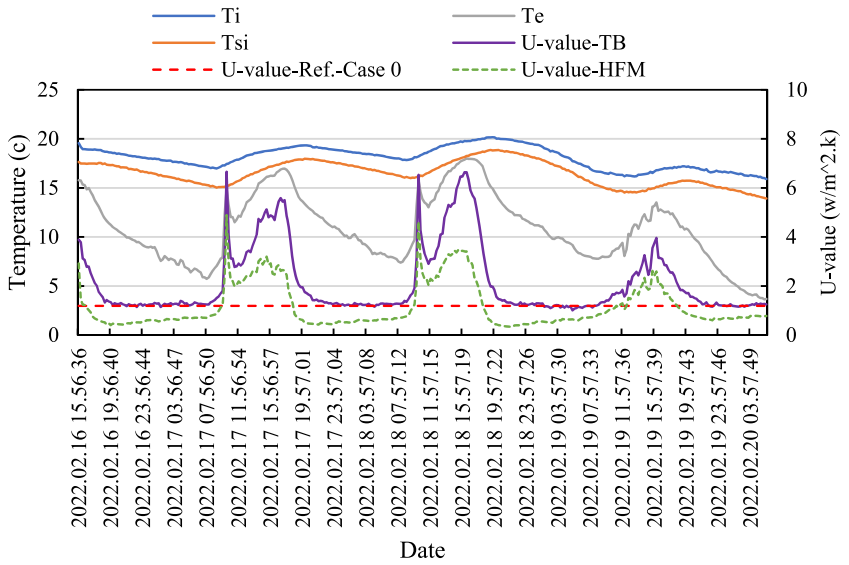

Fig. 11. Time series plots of T_i, T_e, T_{si}, $U-value_{TBM}$, and $U-value_{HFM}$ of the studied building envelope captured by HEAT and the acquired $U-value_{Ref.}$ in the case 0.

635-2, and PT100 devices. A thorough examination of the three figures reveals that the HEAT exterior module experienced direct S.R from 10:00 to 11:00 o'clock, which resulted in rapid increases in both the $U-value_{TBM}$, and $U-value_{HFM}$ during sunny days. In this study, to minimize indoor temperature fluctuations and enhance monitoring accuracy, particularly for the HFM, no heating or cooling system was utilized. Consequently, T_{i-HEAT}, $T_{i-PT100}$, and $T_{i-TESTO}$ exhibit a relatively consistent daily indoor temperature pattern.

Based on the information depicted in these three figures, the temperature ranges detected by the three monitoring systems were as follows: for T_i, it ranged from 15.90 °C to 20.17 °C for HEAT, from 15.80 °C to 20.02 °C for PT100, and from 16.00 °C to 19.90 °C for TESTO. The monitored ranges for T_{si} were 13.92 °C–18.86 °C for HEAT, 14.28 °C–19.03 °C for PT100, and 14.30 °C–19.10 °C for TESTO. Due to the geographical location of the monitored building, the weather conditions during the monitoring period were highly unstable, resulting in significant outdoor temperature variations of up to 14.5 °C. The temperature ranges for T_e were 3.64 °C–18.01 °C for HEAT, 4.67 °C–18.65 °C for PT100, and 4.40 °C–18.90 °C for TESTO.

The fluctuations in interior and exterior temperatures have a significant impact on the calculation of the U-value. Neglecting the impact of these temperature variations can introduce a considerable level of uncertainty about the final results. Consequently, it is important to consider a post-processing technique for the data that involves selecting appropriate ΔT and analyzing the density of the corresponding U-value. By implementing data filtration in the IoT platform and Excel sheet, it was possible to establish a certain condition for ΔT, enabling the identification of its influences on U-values. Furthermore, the placement of outdoor modules in the windowsill and jamb, the exposure to S.R on the sensors, and the duration of W·H had a specific influence on the in-situ U-value

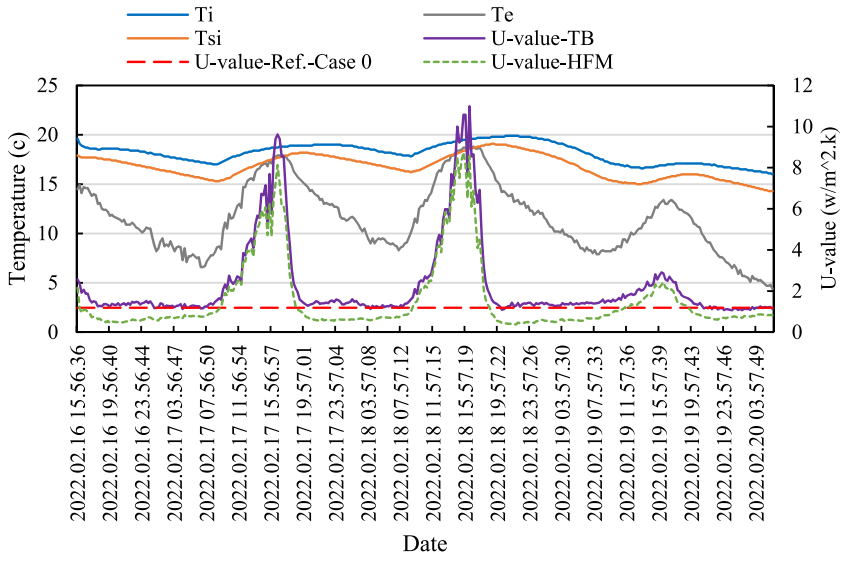

Fig. 12. Time series plots of T_i, T_e, T_{si}, $U-value_{TBM}$, and $U-value_{HFM}$ of the studied building envelope captured by TESTO 635-2 and the acquired $U-value_{Ref.}$ in the case 0.

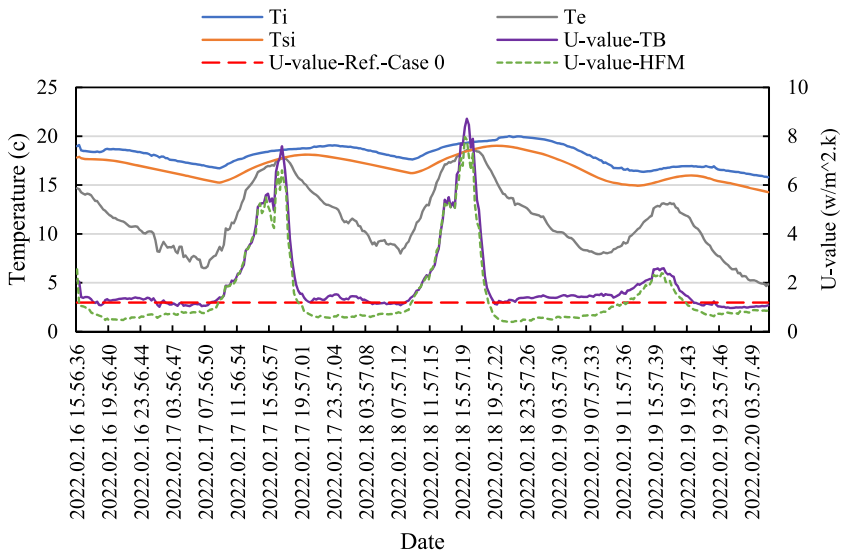

Fig. 13. Time series plots of T_i, T_e, T_{si}, $U-value_{TBM}$, and $U-value_{HFM}$ of the studied building envelope captured by PT100 and the acquired $U-value_{Ref.}$ in the case 0.

calculation. For instance, this can be illustrated by a scenario where the wind speed changed from 0 to 6.8 m/s at 10:00 on February 17, 2022, resulting in a temperature fluctuation of 1.27 °C. To assess the impact of meteorological factors on the performance of both the TBM and HFM approaches, the hourly weather data was collected from the Peñagrande station in Madrid, located approximately 3.4 km away from the monitored building. Fig. 14 displays the variation in wind speed observed throughout the monitoring period.

As depicted in Fig. 14, there was a significant variation in the wind conditions during the survey period, particularly between 11:00 a.m. and 6:00 p.m. During these hours, the wind speed fluctuated between transient values of up to 6.8 m/s and near-zero speeds. In contrast, during the remaining recording hours, the wind speed ranged between a minimum of 0.0 m/s and a maximum of 2.68 m/ s, as shown in Fig. 15. It is worth noting that the HEAT sensor exhibited greater differences in outdoor temperature measurements. This can be attributed to the fact that the HEAT's exterior module, located on the windowsill, was more exposed to solar radiation and varying wind speeds. On the other hand, the TESTO and PT100 outdoor temperature sensors, positioned on the side jamb, were comparatively more protected from these factors.

To examine the simultaneous performance of the TBM and HFM approaches when the outdoor modules are placed in inappropriate locations, a comprehensive investigation was conducted on the recorded temperature parameters. The results obtained for this

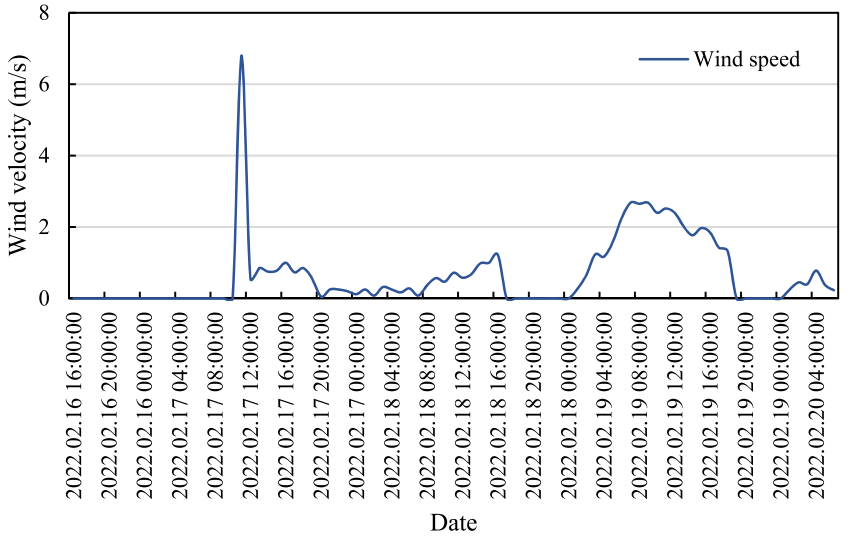

Fig. 14. Wind speed during the monitoring campaign derived from the station of Peñagrande in Madrid.

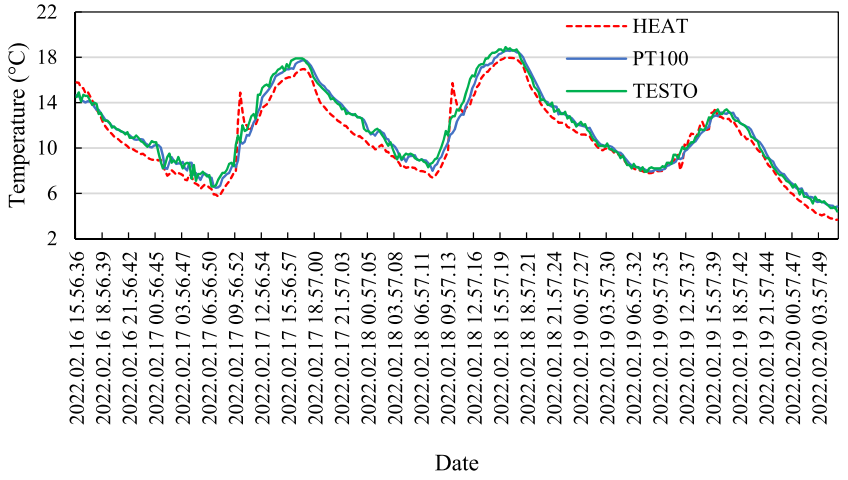

Fig. 15. Exterior temperature comparative.

particular scenario, referred to as case 0, are presented in Figs. 16 and 17 for the TBM and HFM approaches, respectively. Fig. 16(a), (e), and (i) display the number of data points associated with the variations in ΔT, for the data obtained from $HEAT_{TBM}$, $TESTO_{TBM}$, and $PT100_{TBM}$, respectively. Fig. 16(b), (f), and (j) showcase box and whisker plots representing the measurements from $HEAT_{TBM}$, $TESTO_{TBM}$, and $PT100_{TBM}$, respectively. The red lines in these figures indicate the position of the $U - value_{Ref.}$ for case 0. Additionally, Fig. 16(c), (g), and (k) display the differences (ΔU) between the experimental U-values and their corresponding $U - value_{Ref.}$, before and after the removal of outliers resulting from W·H and S.R for $HEAT_{TBM}$, $TESTO_{TBM}$, and $PT100_{TBM}$ measurements, respectively. Lastly, Fig. 16(d), (h), and (l) present the number of identified outliers associated with W·H and S.R for each decrement in ΔT, along with the reduction in ΔU, for the measurements obtained from $HEAT_{TBM}$, $TESTO_{TBM}$, and $PT100_{TBM}$, respectively.

Fig. 17(a), (c), and (e) display box and whisker plots representing the measurements obtained from $HEAT_{HFM}$, $TESTO_{HFM}$, and $PT100_{HFM}$, respectively. The red lines in these figures indicate the position of the $U - value_{Ref.}$ calculated in case 0. On the other hand, Fig. 17(b), (d), and (f) illustrate the ΔU before and after the removal of outliers introduced by W·H and S.R for the measurements recorded by $HEAT_{HFM}$, $TESTO_{HFM}$, and $PT100_{HFM}$, respectively.

5.2.2. Cases 1, 2, and 3

Table 5 displays the U-value ranges obtained at various stages of the ΔT, along with the uncertainty analysis, for the case 1, 2, and 3. In the table, we present three cases:

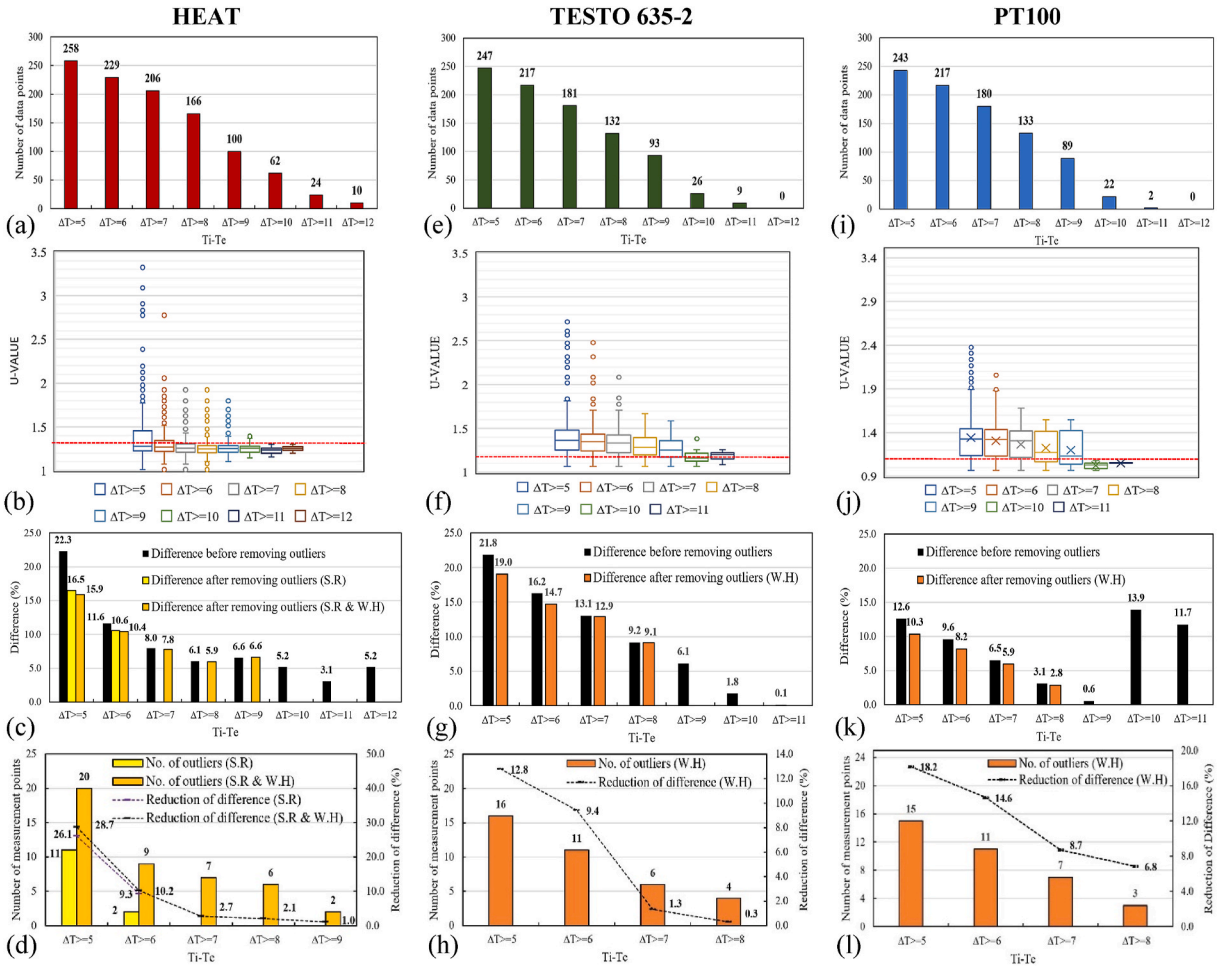

Fig. 16. Analysis of the measurements derived from HEAT ((a), (b), (c), and (d)), TESTO 635-2 ((e), (f), (g), and (h)), and PT100 ((i), (j), (k), and (l)) on the basis TBM approach (case 0).

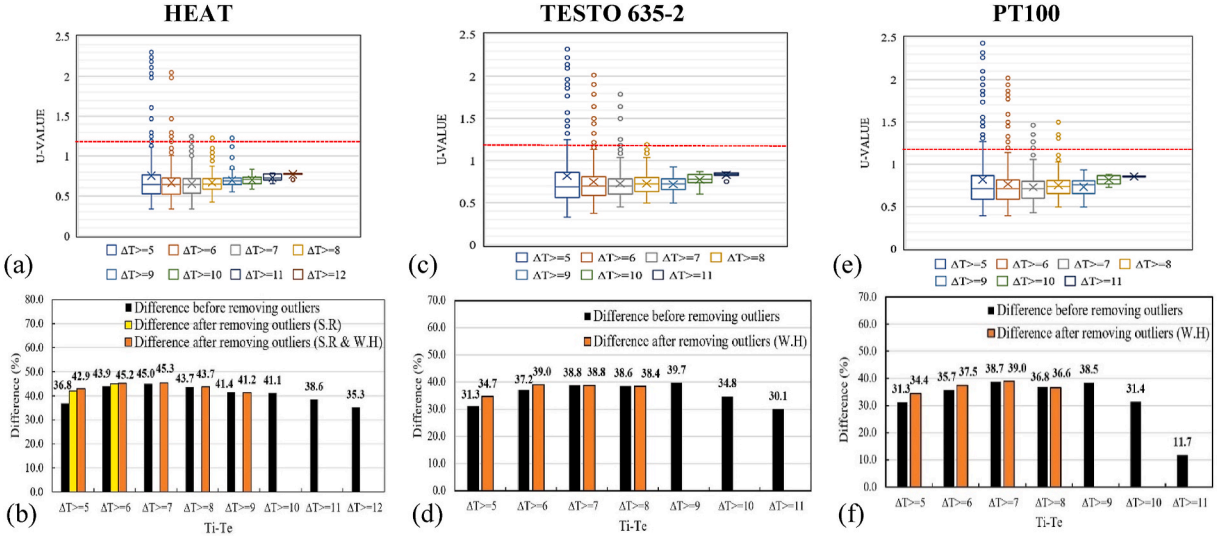

Fig. 17. Analysis of the measurements derived from HEAT ((a) and (b)), TESTO 635-2 ((c) and (d)), and PT100 ((e) and (f)) on the basis HFM approach (case 0).

Table 5
Results of the U-values through TBM (the cases 1, 2, and 3).

ΔT (°C)	Average U-value (W/m².K)								
	Case								
	1			2			3		
	HEAT	PT100	TESTO	HEAT	PT100	TESTO	HEAT	PT100	TESTO
$\Delta T > 0$	1.42 ± 0.92	1.33 ± 1.04	1.52 ± 1.34	1.31 ± 0.85	1.23 ± 0.96	1.40 ± 1.23	1.14 ± 0.74	1.07 ± 0.84	1.22 ± 1.07
$\Delta T \geq 1$	1.42 ± 0.92	1.19 ± 0.75	1.36 ± 1.03	1.31 ± 0.85	1.09 ± 0.69	1.25 ± 0.95	1.14 ± 0.74	0.96 ± 0.60	1.10 ± 0.83
$\Delta T \geq 2$	1.37 ± 0.84	1.01 ± 0.38	1.11 ± 0.47	1.26 ± 0.77	0.93 ± 0.35	1.02 ± 0.44	1.10 ± 0.68	0.81 ± 0.30	0.59 ± 0.38
$\Delta T \geq 3$	1.18 ± 0.57	0.97 ± 0.30	1.04 ± 0.34	**1.08 ± 0.52**	0.90 ± 0.28	0.96 ± 0.31	**0.95 ± 0.45**	0.78 ± 0.24	0.84 ± 0.27
$\Delta T \geq 4$	**1.08 ± 0.44**	0.92 ± 0.22	1.00 ± 0.27	1.00 ± 0.40	0.85 ± 0.20	0.92 ± 0.25	0.87 ± 0.35	0.74 ± 0.18	0.81 ± 0.22
$\Delta T \geq 5$	0.97 ± 0.30	0.89 ± 0.18	0.97 ± 0.23	0.89 ± 0.26	0.82 ± 0.17	0.89 ± 0.21	0.78 ± 0.24	0.72 ± 0.15	0.78 ± 0.18
$\Delta T \geq 6$	0.89 ± 0.15	0.87 ± 0.14	0.92 ± 0.15	0.82 ± 0.13	0.80 ± 0.13	0.85 ± 0.14	0.71 ± 0.12	0.70 ± 0.11	0.74 ± 0.12
$\Delta T \geq 7$	0.86 ± 0.09	0.85 ± 0.12	0.90 ± 0.12	0.79 ± 0.08	0.78 ± 0.11	0.83 ± 0.11	0.69 ± 0.07	0.68 ± 0.09	0.72 ± 0.09
$\Delta T \geq 8$	0.84 ± 0.08	0.82 ± 0.12	0.87 ± 0.09	0.77 ± 0.07	0.75 ± 0.11	0.80 ± 0.08	0.68 ± 0.06	0.66 ± 0.09	0.70 ± 0.07
$\Delta T \geq 9$	0.85 ± 0.07	0.80 ± 0.13	0.84 ± 0.08	0.78 ± 0.07	0.73 ± 0.12	0.78 ± 0.07	0.68 ± 0.06	0.64 ± 0.10	0.68 ± 0.06
$\Delta T \geq 10$	0.84 ± 0.04	0.68 ± 0.02	0.78 ± 0.05	0.77 ± 0.03	0.63 ± 0.02	0.72 ± 0.04	0.67 ± 0.03	0.55 ± 0.01	0.63 ± 0.04
$\Delta T \geq 11$	0.82 ± 0.03	1.05 ± 0.01	0.79 ± 0.03	0.75 ± 0.02	1.05 ± 0.01	0.73 ± 0.03	0.66 ± 0.02	1.05 ± 0.01	0.64 ± 0.03
$\Delta T \geq 12$	0.84 ± 0.02			0.77 ± 0.02			0.67 ± 0.01		

- In case 1, the U-value estimations for the three monitoring systems were conducted considering the design parameters obtained from the measurements of the PT100 system.
- In case 2, the U-value estimations for the three monitoring systems were carried out considering the design parameters obtained from the measurements of the TESTO system.
- In case 3, the U-value estimations for the three monitoring systems were performed considering the design parameters obtained from the measurements of the HEAT system.

Based on the information in this table, the U-value obtained from an individual monitoring system differs for each level of the $\Delta T \geq X$ °C pattern. For example, as the ΔT increases from 0 to 12 °C, the U-values calculated by the HEAT system change as follows for cases 1, 2, and 3: from 1.42 ± 0.92 to 0.84 ± 0.02, from 1.31 ± 0.85 to 0.77 ± 0.02, and from 1.14 ± 0.74 to 0.67 ± 0.01, respectively. Similarly, when considering the PT100 system, the measured U-values change from 1.33 ± 1.04 to 1.05 ± 0.01, from 1.23 ± 0.96 to 1.05 ± 0.01, and from 1.07 ± 0.84 to 1.05± 0.01. Lastly, for the TESTO measurements, the U-values vary from 1.52 ± 1.34 to 0.79 ±

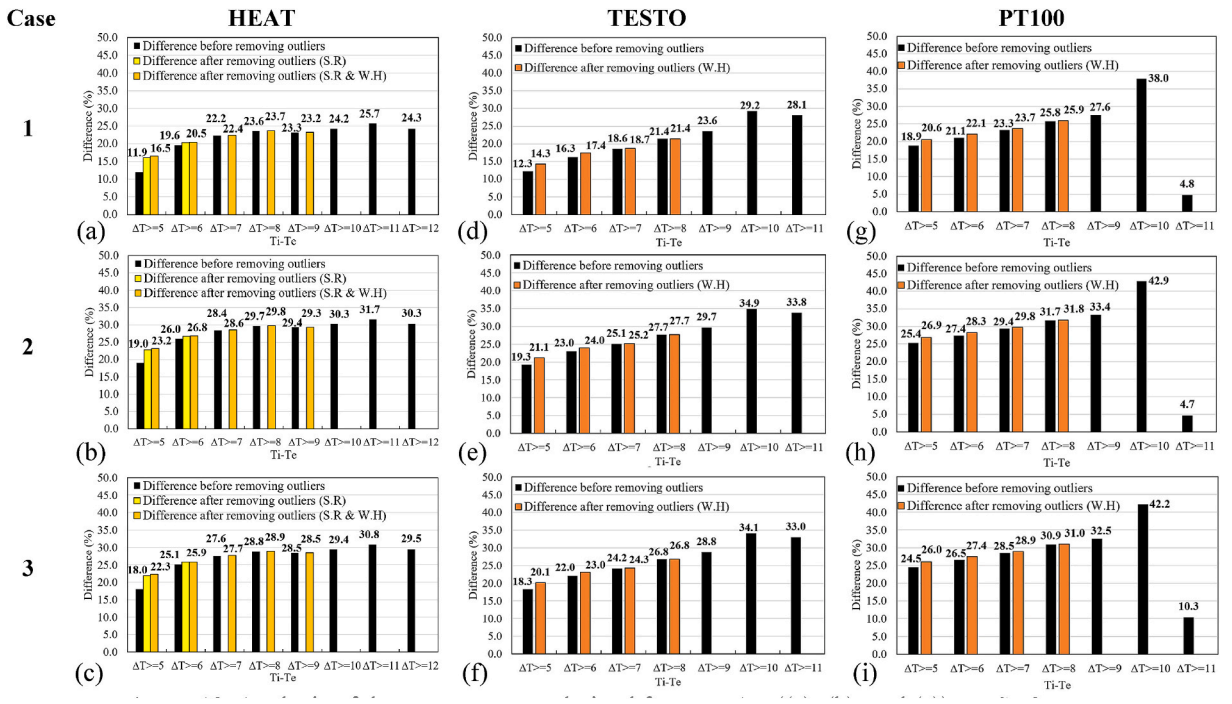

Fig. 18. Analysis of the measurements derived from HEAT ((a), (b), and (c)), TESTO 635-2 ((d), (e), and (f)), and PT100 ((g), (h), and (i)) on the basis TBM approach (cases 1, 2, and 3).

0.03, from 1.40 ± 1.23 to 0.73 ± 0.03, and from 1.22 ± 1.07 to 0.64 ± 0.03.

Fig. 18 illustrates the variations in ΔU both before and after the removal of outliers generated from the W·H and S.R for cases 1, 2, and 3. Specifically, Fig. 18(a), (b), and (c) represent the outcomes of the HEAT device for cases 1, 2, and 3, respectively. Likewise, Fig. 18(d), (e), and (f) correspond to the results obtained from the TESTO device for cases 1, 2, and 3, respectively. Finally, Fig. 18(g), (h), and (i) depict the outcomes of the PT100 device for cases 1, 2, and 3, respectively.

6. Discussion

In this section, a comprehensive discussion is provided regarding the results presented in the previous chapter concerning the TBM and HFM approaches in various cases.

6.1. Case 0

When a heating system is operating in the monitoring room, the direct approach (HFM) results in an uneven enhancement of the heat flux rate, leading to higher instantaneous U-values compared to the indirect approach (TBM) [67]. Conversely, when the convective thermal energy is attenuated due to the heating system being turned off, the heat flux measured by the heat flux sensor decreases, resulting in lower U-values for the HFM approach compared to the TBM approach. Considering this fact, along with the raw data presented in Table 4 and the U-value patterns depicted in Figs. 11–13, it can be seen that the TBM monitoring systems yielded a wider range of U-values compared to the HFM systems. As a consequence, the TBM approaches ($HEAT_{TBM}$ = 74.59%, $PT100_{TBM}$ = 69.52%, and $TESTO_{TBM}$ = 71.43%) exhibited a greater reduction in U-values compared to the HFM approaches ($HEAT_{HFM}$ = 58.90%, $PT100_{HFM}$ = 52.33%, and $TESTO_{HFM}$ = 67.47%) as the ΔT increased from 1 to 11 °C. This observation aligns with the results presented in Fig. 19, which provides a comparison of heat flux densities derived from the heat flux sensor and TBM monitoring systems. The results depicted in Fig. 19 highlight that the heat flux density obtained directly from the heat flux sensor (2.50 $W/m^2 \leq q_{HFM} \leq$ 12.50 W/m^2) exhibits a lower range compared to the heat flux densities calculated by the TBM monitoring systems (8.61 $W/m^2 \leq HEAT_{TBM} \leq$ 17.69 W/m^2, 4.31 $W/m^2 \leq PT100_{TBM} \leq$ 14.76 W/m^2, and 5.38 $W/m^2 \leq TESTO_{TBM} \leq$ 15.38 W/m^2).

From a theoretical perspective, achieving a constant ΔT is necessary to prevent the influence of thermal gradient variations. However, achieving temperature stability during on-site investigations is challenging, particularly in dry Mediterranean climates. As a result, a preliminary data analysis was conducted in 12 stages, considering variations in the ΔT.

Fig. 16(a), (e), and (i) present information on the number of data points obtained when applying the $\Delta T \geq X$°C pattern to the U-value measurements conducted by the HEAT, TESTO, and PT100 systems, respectively. Based on these figures, as the temperature difference is increased from $\Delta T \geq 5$°C to $\Delta T \geq 12$°C, the number of data points decreases from 258 to 10 in Fig. 16(a) for the HEAT system, from 247 to 0 in Fig. 16(e) for the TESTO system, and from 243 to 0 in Fig. 16(i) for the PT100 system. Fig. 16(b), (f), and (j) show statistical information for $HEAT_{TBM}$, $TESTO_{TBM}$, and $PT100_{TBM}$, respectively, providing descriptive characteristics of U-values as well as identifying outliers resulting from improper sensor positioning. As anticipated, the system with lower sensor accuracy (HEAT) produced a broader distribution of data points compared to the more accurate systems (TESTO and PT100). Furthermore, the improved precision of the instruments is evident in the reduced range of differences observed between TESTO and PT100, with the PT100 being the most precise and having the narrowest range of data point. For instance, when considering a temperature difference of $\Delta T \geq 5$°C, the monitoring systems showed ranges of U-values as follows: 1.01 $W/m^2.K \leq HEAT_{TBM} \leq$ 3.32 $W/m^2.K$, 1.07 $W/m^2.K \leq TESTO_{TBM} \leq$ 2.75 $W/m^2.K$, and 0.97 $W/m^2.K \leq PT100_{TBM} \leq$ 2.38 $W/m^2.K$. In essence, the higher dispersion of U-values measured by the HEAT system can also be attributed to the impact of direct solar radiation on the HEAT exterior module. Nonetheless, the box and whisker plots demonstrate a significant reduction in uncertainties when the $\Delta T \geq X$°C pattern was applied. Considering the range between the first quartile and third quartile as well as the presence of potential outliers, it can be concluded that a temperature difference of $\Delta T \geq 9$°C yields more consistent U-value measurements for TESTO and PT100 in case 0. However, in the case of the HEAT system, a higher temperature difference such as $\Delta T \geq 10$°C is required to obtain the most compatible U-value measurements. As shown in Fig. 16(c), (g), and (k), applying the $\Delta T \geq X$°C pattern in TBM approaches resulted in a downward trend in the ΔU (indicated by the black bars). It is important to note that an increase in the ΔT from 9 to 10 °C resulted in a significant reduction in the number of data points, subsequently impacting the corresponding U-values. This phenomenon is particularly noticeable in the cases of the TESTO and PT100 devices, as indicated in Fig. 16(g) and (k). The decrease in the number of data points by 72% and 75% for TESTO and PT100 devices, respectively, led to a sudden decrease and increase in ΔU, from 6.1% to 1.8% for $TESTO_{TBM}$ and from 0.6% to 13.9% for $PT100_{TBM}$. These findings, in conjunction with the box and whisker plots, confirm the methodology adopted for the data post-processing in the preliminary stage. The impact of S.R on the exterior sensors was found to be a significant factor causing notable variations in the measured T_e. Therefore, a secondary data filtration process was implemented specifically for the S.R on the sensors. To eliminate the influence of this parameter, only the data collected from the HEAT system was considered, as it was the only set of sensors directly exposed to solar radiation during the monitoring campaign. Fig. 16(c) illustrates the effect of solar radiation, which was observed only in the data points categorized under $\Delta T \geq 5$ and 6 °C. By excluding these data points, more stable environmental conditions were achieved, enabling a more accurate estimation of the U-value (depicted by the yellow bars). Fig. 16(c) demonstrates that by removing data points recorded during direct S.R exposure on the exterior module, the ΔU s corresponding to the $\Delta T \geq 5$ °C and $\Delta T \geq 6$ °C categories decreased from 22.3% to 16.5% and from 11.6% to 10.6%, respectively. This means that the elimination of 11 and 2 outliers in the aforementioned categories, as depicted by the purple line in Fig. 16(d), resulted in a reduction of differences by 26.1% and 9.3% respectively.

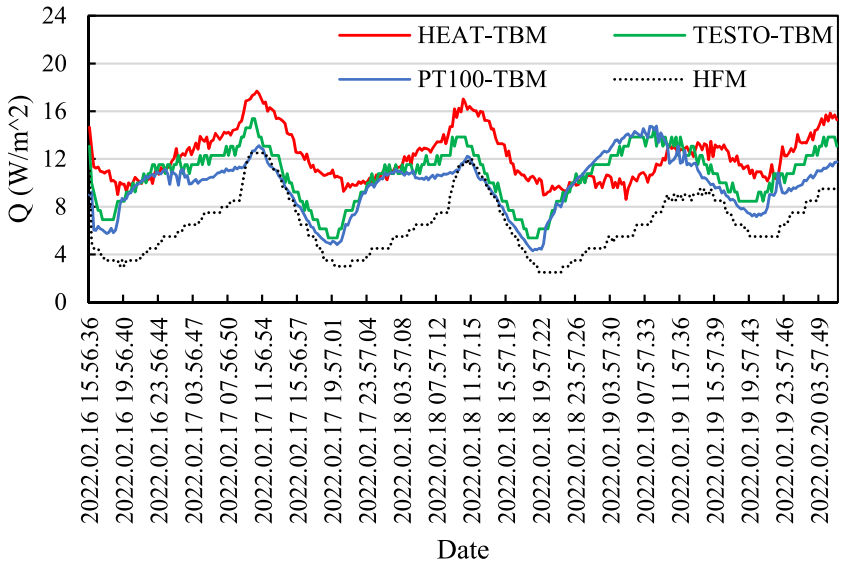

Fig. 19. Comparison between heat fluxes derived from flux sensor, and the TBM monitoring devices.

Considering the fluctuating weather conditions in the climate zone under study, the final step involved post-processing the data in relation to W.H. A visual examination of Fig. 16(c), (g), and (k) demonstrates the efficacy of the data elaboration based on weather changes in obtaining a more accurate and representative U-value for the investigated wall using TBM approaches. The process of outlier detection was applied to the data points grouped from $\Delta T \geq 5$°C up to the $\Delta T \geq 9$°C for the measurements of $HEAT_{TBM}$, and up to $\Delta T \geq 8$°C for both $TESTO_{TBM}$ and $PT100_{TBM}$. By considering both S.R and W·H, the orange bars in Fig. 16(c) demonstrate the evolution of ΔU for the fully post-processed U-value obtained from $HEAT_{TBM}$. This figure illustrates that by removing all the outliers, the ΔU decreased by 58%, from $\Delta T \geq 5$°C (15.9%) to $\Delta T \geq 9$°C (6.6%). Further analysis (Fig. 16(d)) reveals that the detection and elimination of 20, 9, 7, 6, and 2 outliers resulted in reductions of ΔU in $HEAT_{TBM}$ by 28.7%, 10.2%, 2.7%, 2.1%, and 1%, respectively. Fig. 16(e) and (i) present the number of data points at different stages of ΔT corresponding to the TESTO and PT100 monitoring systems, respectively. Moreover, Fig. 16(h) and (l) present the reduction of ΔU when removing the outliers, corresponding to the measurements of TESTO and PT100 monitoring systems, respectively. Based on Fig. 16(g) and (h), for the $TESTO_{TBM}$ measurements, the removal of 16, 11, 6, and 4 outliers resulted in reductions of ΔU by 19.0%, 14.7%, 12.9%, and 9.1%, respectively. Similarly, as shown in Fig. 16(K) and (l), for the $PT100_{TBM}$ measurements, the elimination of 15, 11, 7, and 3 outliers led to decreases in ΔU by 10.3%, 8.2%, 5.9%, and 2.8%, respectively.

The observed variations of ΔUs indicate that the reduction of ΔU was not consistent across the three monitoring systems in case 0 during the data processing. This discrepancy can be attributed to the varying precision of the sensors used in each monitoring system, resulting in different quantities of data points when applying the condition $\Delta T \geq$ X °C. For example, when implementing the $\Delta T \geq$ 10°C condition, the number of data points recorded by the HEAT system was more than twice that of the TESTO and PT100 systems. Essentially, the limited number of data points available at this stage significantly affected the trend of ΔU for both the $TESTO_{TBM}$ and $PT100_{TBM}$. Consequently, a preliminary conclusion regarding the results of the TBM approaches suggests that insufficient data points can be a weakness but is a common challenge in the in-situ U-value measurement. In this investigation an approximate number of 100 data points was considered to estimate the U-value. Therefore, an average U-value of 1.24 W/m^2.K was achieved in the Case 0. This value represents the average of the U-values recorded by three monitoring systems. The suggested U-value demonstrates strong agreement with the corresponding $U - value_{Ref.}$ as it exhibits a difference of less than 4.5%. A precise analysis of individual U-values further confirms the effectiveness of the proposed data processing methodology, as differences of 6.6%, 6.1%, and 0.6% obtained for $HEAT_{TBM}$, $TESTO_{TBM}$, and $PT100_{TBM}$, respectively.

Key features of the distributions associated with the measurements of $HEAT_{HFM}$, $TESTO_{HFM}$, and $PT100_{HFM}$, can be observed in Fig. 17(a), (c), and (e), respectively. When comparing the two adopted approaches (TBM and HFM) using the information of the box and whisker plots, it is evident that the interquartile ranges, which represent the middle 50% of U-values, were situated at different ranges. In the TBM approach, the interquartile range spanned from 0.98 to 1.48 W/m^2.K, whereas in the HFM approach, it ranged from 0.52 to 0.87 W/m^2.K.

Regarding the $HEAT_{HFM}$ measurements (Fig. 17(a)), for all $\Delta T \geq$ X°C conditions, the $U - value_{Ref.}$ shows a notable deviation from the mean value, lying beyond the upper whisker of the box plot. This indicates that data points close to the reference U-value may be considered as potential outliers. As a result, it can be observed that the $HEAT_{HFM}$ exhibits a higher level of ΔU. Furthermore, the $U - value_{Ref.}$ was barely matched by just the initial two boxes of $PT100_{HFM}$ ($\Delta T \geq 5$°C and $\Delta T \geq 6$°C) and the first box of $TESTO_{HFM}$ ($\Delta T \geq 5$°C). Based on the information provided above, the utilization of the pattern not only failed to reduce the uncertainties associated with the HFM approaches but increased the ΔU in certain instances, particularly when the temperature difference reached or exceeded 7 °C. Thus, the analysis of the results suggests that the HFM approaches (depicted in Fig. 17(b), (d), and (f)) exhibit a

Table 6
Impact of an individual outlier on the reduction of ΔU in TBM and HFM approaches (case 0).

ΔT (°C)	Case 0											
	TBM						HFM					
	HEAT		PT100		TESTO		HEAT		PT100		TESTO	
	No.*	Imp.** (%)	No.	Imp. (%)	No.	Imp. (%)	No.	Imp. (%)	No.	Imp. (%)	No.	Imp. (%)
≥ 5°C	20	1.4	15	0.5	16	0.8	20	–	15	–	16	–
≥ 6°C	9	1.1	11	1.3	11	0.9	9	–	11	–	11	–
≥ 7°C	7	0.4	7	1.2	6	0.2	7	–	7	–	6	–
≥ 8°C	6	0.5	3	2.3	4	0.1	6	0.1	3	1.8	4	0.9
≥ 9°C	2	0.5	–	–	–	–	2	0.2	–	–	–	–

* No.: Number of outliers.
** Imp.: Impact of an individual outlier.

higher level of ΔU compared to the TBM approaches (depicted in Fig. 16(c), (g), and (k)). Furthermore, the pattern of changes in ΔU was different in HFM compared to the TBM approach, as the data elaboration resulted ascending and descending order of variation in the former. For example, in Fig. 17(b), the secondary data filtering based on the S.R. resulted in an increase in ΔU for the $HEAT_{HFM}$ in both categories: $\Delta T \geq 5$ °C (rising from 36.8% to 42.1%) and $\Delta T \geq 6$ °C (increasing from 43.9% to 44.9%). Moreover, upon eliminating outliers related to both the S.R and W·H, the ΔU s for the $HEAT_{HFM}$ changed from 36.8%, 43.9%, 45.0%, 43.7%, and 41.4%–42.9%, 45.2%, 45.3%, 43.7%, and 41.2%, respectively.

When a suitable number of data points were considered for estimating the U-value using the HFM approach at the $\Delta T \geq 9$ °C stage, an average U-value of 0.72 $W/m^2.K$ was obtained, with a ΔU of 39.8%. In order to provide a clearer understanding of the connection between the test conditions, sensor placement, and data post-processing, Table 6 provides details on how individual outliers affect the decrease in ΔU for both TBM and HFM approaches at various $\Delta T \geq X$ °C stages in case 0. An overall impression is that TBM systems demonstrated superior performance compared to HFM systems when post-processing of the data was carried out. When comparing these two approaches, notable improvements in U-value estimation were observed across all ΔT stages for TBM monitoring systems. Conversely, HFM approaches showed gradual improvements when the recorded nocturnal data was post processed. The majority of data linked to the $\Delta T \geq 8$ °C, was obtained during nighttime. Prior to the removal of outliers, approximately 84%, 79%, and 82% of the total hours with this temperature difference occurred between 8:00 p.m. and 8:00 a.m. The findings presented in Table 6 also suggest that monitoring systems with higher levels of accuracy were more susceptible to the influence of outliers. This can be observed by examining the impact of individual outliers on the attenuation of ΔU in TBM systems. According to this table, the most accurate monitoring systems exhibited a wider range of impact, ranging from 1.2% to 2.3% for $PT100_{TBM}$, while the least accurate system showed a narrower range of impact, ranging from 0.4% to 1.4% for $HEAT_{TBM}$. A similar trend was observed for HFM systems, where the removal of a single outlier in PT100_HFM resulted in a 1.8% reduction in ΔU. On the other hand, eliminating a single outlier in the case of HEAT_HFM led to a mere 0.1% reduction in ΔU.

6.2. Cases 1, 2, and 3

When comparing the four cases to each other, significant differences were evident in the obtained results, indicating diverse ranges of U-values as well as varying levels of uncertainty. This situation can be easily understood by examining the results presented in Tables 4 and 5 For example, in relation to the measurements taken by the TBM (Table 4), case 0 demonstrated a greater U-value and uncertainty ($1.25 \pm 0.03 \leq HEAT_{case\ 0} \leq 2.13 \pm 1.38$) compared to the other cases (Table 5), such as case 1 ($0.84 \pm 0.02 \leq HEAT_{case\ 1} \leq 1.42 \pm 0.92$), case 2 ($0.77 \pm 0.02 \leq HEAT_{case\ 2} \leq 1.31 \pm 0.85$), and case 3 ($0.67 \pm 0.01 \leq HEAT_{case\ 3} \leq 1.14 \pm 0.74$). The reason for the higher U-value observed in case 0 can be attributed to the fact that the heat transfer coefficient assumed by the CTE was greater than the ones obtained from the measurements of the three monitoring systems (Table 3). Fig. 18 illustrates a comparison between the U-values obtained from three monitoring systems and the reference U-value for their respective cases. When comparing the findings presented in Fig. 16 with Fig. 18, it becomes evident that the data filtration process in cases 1, 2, and 3 led to a deterioration in the agreement between the measured U-values and their corresponding $U - value_{Ref.}$. The degradation of the results in relation to ΔU can be attributed to the fact that the measurements for the internal and external surface resistances of the wall were supposed to be taken under specific conditions, where the exterior temperature is 10 °C, interior temperature is 20 °C, and exterior wind speed is 4 m/ s. However, due to limitations in the monitoring campaign, it was not possible to achieve these conditions. Under such circumstances, the $U - value_{Ref.}$ obtained for cases 1, 2, and 3 were in proximity to the U-values of their respective cases at the third or fourth stages of the $\Delta T \geq X$°C pattern (*e.g.*, bold values in Table 5). Consequently, it can be observed that as the ΔT increased, a corresponding increase in ΔU was also observed. However, Table 5 emphasizes that when assessing the U-value of the wall without considering the role of the $U - value_{Ref.}$, the consistency of the measurements was achieved based on the temperature difference. Therefore, keeping this in mind, characterizing the U-value of the wall using the in-situ measurements of h_{in} (Table 5) resulted in a lower range of uncertainty compared to case 0.

As depicted in Fig. 18, it is important to note that the trends observed for the three cases confirm the significance of sensor accuracy in obtaining reliable values. Specifically, in case 1, where the h_{in} values were measured using the most accurate sensor device, the

lowest level of ΔU was achieved compared to cases 2 and 3. In case 1, after removing the outliers at the $\Delta T \geq 9$ °C stage, the minimum and maximum ΔU values were 23.2% (HEAT) and 27.6% (PT100), respectively. On the other hand, in case 3, where the h_{in} values were measured using the HEAT system, the ΔU at the same stage as case 1 ranged from 28.5% (HEAT) to 32.5% (PT100). Based on the information provided in Figs. 16 and 17, the deviations varied between 0.6% and 6.6% in case 0 when estimating the U-value using the TBM approach. However, when the HFM approach was used for U-value characterization, the deviations ranged from 38.5% to 41.2%. Additionally, in cases 1, 2, and 3, the deviations spanned from 23.2% to 27.6%, 29.3%–33.4%, and 28.5%–32.5%, respectively, as shown in Fig. 18.

Indeed, the findings of this research align closely with a previous study conducted in Korea, which focused on thermal monitoring of four case studies at various measurement points using the TBM approach [7]. The monitoring assumption made in the aforementioned study was similar to the one employed in this research for case 0, where the design parameter was set as $h_{in} = 7.69\ W/m^2.K$. The results obtained in the previous study exhibited comparable ranges of deviations to the current research, ranging from 0.6% to 6.6%, 1.42%–4.44%, 2.37%–4.69%, 2.44%–4.64%, and 0.28%–4.56%.

Regarding the HFM approach, a separate study conducted in Italy yielded distinct deviations compared to the present research (ranging from 38.5% to 41.2%). This particular survey was carried out under steady state monitoring conditions, resulting in lower deviations. The obtained ranges of deviations in that study were from 33 to 36% for the first location of the heat flux sensors and from 23 to 26% for the second and third locations [44].

In another case study conducted in Canada, the researchers aimed to determine the U-values of three walls using IRT [46]. The study revealed that the U-value measurements obtained with IRT, under the most favorable circumstances (depending on the location of the ROI), deviated from the nominal U-values by 6.25%–25.00%. Upon further analysis, the results unveiled deviations ranging from −60.87% to 8.70% for the first wall, deviations of −75.00% to −31.25% for the second wall, and deviations of 25.0%–62.5% for the third wall. The results of this study have practical implications in avoiding inaccurate estimations of building thermal parameters under nonoptimal monitoring conditions. The investigation aimed to examine the effects of test conditions and improper placement of exterior sensors on the accuracy of U-value estimation. By conducting this study on a building with a known envelope stratigraphy, it was possible to assess the range of uncertainty that arises when performing thermal monitoring without prior information about the building elements. Based on the findings, it is crucial to have a thorough understanding of the variables associated with the different approaches used for building characterization, prior to conducting any monitoring. A detailed analysis of the results highlighted that when nonoptimal operative conditions are present, applying the TBM approach while considering design parameters from the standard can yield promising U-value estimations. However, this necessitates robust outlier detection methods which are sensitive to the unfavorable monitoring conditions.

7. Conclusions

This research paper showcased the outcomes of a study focused on the precise characterization of the U-value of a residential building wall, when the placement of outdoor sensors did not meet the optimal conditions specified by standards. To accomplish this, to assess the impact of this circumstance, three monitoring systems with various accuracies and operational methods were utilized. These systems were employed to quantify the level of uncertainty arising from this particular factor, in relation to both the TBM and HFM approaches. The results obtained from the study revealed that: (1) The impact of positioning the exterior sensors at the window sill and jamb was not similar for the outcomes obtained through the TBM and HFM approaches. After postprocessing the monitoring data, the TBM approach demonstrated a greater improvement in accuracy compared to the HFM approach. Specifically, for the most accurate system, PT100, deviations of 0.6% and 38.5% were observed respectively, for the U-values estimated using the TBM and HFM approaches. (2) Under non-steady climate conditions, the design parameters (R_{si}, R_{se}, and h_{in}) specified by the standards demonstrated relatively lower deviations between the reference U-value measurements and the in-situ U-value measurements, compared to the U-values estimated using the design parameters measured on-site. For case 0, when considering the stage of $\Delta T \geq 9$°C, the deviations of U-values ranged from 0.6% to 6.6%. In contrast, for case 1, the deviations varied from 23.2% to 27.6%, for case 2 they ranged from 29.3% to 33.4%, and for case 3 they spanned from 28.5% to 32.5%. (3) There existed a correlation between the magnitude of ΔT and the quantity of data points required for accurate U-value characterization. As the ΔT increased from 9 to 10 °C, there was a sudden decrease in the number of data points available, which subsequently influenced the resulting U-values. The reduction in data points by 72% and 75% led to a significant decrease and increase in deviations. For the U-value measured by the TESTO system, the deviation was decreased from 6.1% to 1.8%. Conversely, for the U-value measured by the PT100 system, the deviation was increased from 0.6% to 13.9%.

Indeed, this study encountered two limitations, which are outlined as follows: (a) Challenges in simultaneously characterizing the investigated wall under both optimal and nonoptimal positioning of the outdoor sensors. This study faced the constraint of not having access to the back side of the investigated wall. As a result, the case study was limited to installing the exterior sensors solely in the windowsill and jamb. Consequently, the deviation of the results could only be compared against the reference U-values provided by the CTE standard, rather than against a standard wall instrumentation scenario. (b) The absence of facilities to mitigate the impact of measurement location and boundary conditions was another limitation of this study. To avoid thermal bridges, interior sensors were traditionally installed in the center of the wall. However, the placement of heat flux and indoor surface temperature sensors required careful investigation to ensure thermal homogeneity, absence of thermal bridges, air leakages, moisture, and cracks.

Hence, it is crucial for future studies to study the uncertainty associated with in-situ U-value measurements under improper position of the sensors, considering the results with those obtained from the standard sensor building instrumentation. In this way, it is also recommended to conduct a preliminary analysis of the targeted building element using the state-of-the-art monitoring systems, so

as to determine an appropriate location for sensor placement.

Author contribution statement

Behnam Mobaraki, Miguel Angel Mellado Mascaraque, and Arturo Martínez García - conceived and designed the experiments; analyzed and interpreted the data; contributed reagents, materials, analysis tools or data; performed the experiments; wrote the paper.

Francisco Javier Castilla Pascual; Borja Frutos Vázquez; Carmen Alonso - conceived and designed the experiments; analyzed and interpreted the data; and contributed reagents, materials, analysis tools or data.

Data availability statement

Data will be made available on request.

Declaration of competing interest

The authors declare that they have no known competing financial interests or personal relationships that could have appeared to influence the work reported in this paper.

Acknowledgments

The authors are indebted to the Spanish Ministry of Economy and Competitiveness for the funding provided through the research projects BIA2017-86811-C2-1-R, directed by Jose Turmo, BIA2017-86811-C2-2-R, directed by Jose Antonio Lozano-Galant, and PID2021-126405OB-C32 funded by FEDER funds—A Way to Make Europe and Spanish Ministry of Economy and Competitiveness MICIN/AEI/10.13039/501100011033/. It is also to be noted that funding for this research has been provided to Behnam Mobaraki by Ministerio de Ciencia Innovación y Universidades: grant number: 2018-COB-9092. Arturo Martínez acknowledges the support provided by the Consejo Nacional de Ciencia y Tecnología (CONACYT) and the Fundación del Instituto Nacional de Bellas Artes (FINBA) given through its doctorate scholarship program.

Nomenclature

d	Thickness [m]
HFM	Heat flux meter [−]
HEAT	Hyper efficient Arduino transmittance-meter [−]
IoT	Internet of Things
h_{in}	Internal total heat transfer coefficient [$W/m^2.K$]
q	Heat flux density [W/m^2]
R	Thermal resistance for different layers of the wall [m^2k/W]
$\overline{R}$	Thermal resistance (inverse of thermal conductance) [m^2k/W]
R_{se}	Thermal resistance of exterior surface [m^2k/W]
R_{si}	Thermal resistance of interior surface [m^2k/W]
R_{st}	Total value of surface thermal resistances [m^2k/W]
R_T	Total thermal resistance of the wall [m^2k/W]
S.R	Solar radiation [−]
TBM	Temperature-based method [−]
T_i	Interior air temperature [K, °C]
T_e	Exterior air temperature [K, °C]
T_{si}	Interior surface temperature of envelope [K, °C]
U	Thermal transmittance [$W/m^2.K$]
$U-value_{Ref.}$	Reference U-value [$W/m^2.K$]
$U-value_{HFM}$	U-value on the basis of heat flux meter approach [$W/m^2.K$]
$U-value_{TBM}$	U-value on the basis of temperature-based approach [$W/m^2.K$]
W·H	Windy hour [−]
λ	Thermal conductivity of the material [W/mK]
ΔT	Temperature difference between the interior and exterior [K, °C]

References

[1] B. Tejedor, E. Lucchi, D. Bienvenido-Huertas, I. Nardi, Non-destructive techniques (NDT) for the diagnosis of heritage buildings: traditional procedures and futures perspectives, Energy Build. 263 (2022), 112029, https://doi.org/10.1016/j.enbuild.2022.112029.

[2] Z. Liu, J. Hou, L. Zhang, B.J. Dewancker, X. Meng, C. Hou, Research on energy-saving factors adaptability of exterior envelopes of university teaching-office buildings under different climates (China) based on orthogonal design and EnergyPlus, Heliyon 8 (2022), e10056, https://doi.org/10.1016/j.heliyon.2022.e10056.

[3] E. Lucchi, Diagnosi Energetica Strumentale Degli Edifici. Termografia e Analisi Non Distruttive, ISBN 978-8857901220, Normativa e Procedure Operative, 2012.

[4] M.Á. Mellado Mascaraque, F.J. Castilla Pacual, I. Oteiza, S. Aparicio Secanellas, Hygrothermal assessment of a traditional earthen wall in a dry mediterranean climate, Build. Res. Inf. 48 (2020) 632–644, https://doi.org/10.1080/09613218.2019.1709787.

[5] D. Bienvenido-Huertas, J. Moyano, D. Marín, R. Fresco-Contreras, Review of in situ methods for assessing the thermal transmittance of walls, Renew. Sustain. Energy Rev. 102 (2019) 356–371, https://doi.org/10.1016/j.rser.2018.12.016.

[6] F. Asdrubali, F. D'Alessandro, G. Baldinelli, F. Bianchi, Evaluating in situ thermal transmittance of green buildings masonries: a case study, Case Stud. Constr. Mater. 1 (2014) 53–59, https://doi.org/10.1016/j.cscm.2014.04.004.

[7] S.H. Kim, J.H. Kim, H.G. Jeong, K.D. Song, Reliability field test of the air-surface temperature ratio method for in situ measurement of U-values, Energies 11 (2018) 1–15, https://doi.org/10.3390/en11040803.

[8] International Organization for Standardization ISO 9869, 2014 Thermal Insulation – Building Elements – in Situ Measurement of Thermal Resistance and Thermal Transmittance, 2014.

[9] European Standard EN ISO 8990, Thermal Insulation Determination of Steady State Thermal Transmission Properties Calibrated and Guarded Hot Box, 1996.

[10] A. Rasooli, L. Itard, In-situ characterization of walls' thermal resistance: an extension to the ISO 9869 standard method, Energy Build. 179 (2018) 374–383, https://doi.org/10.1016/j.enbuild.2018.09.004.

[11] M. Teni, H. Krstić, P. Kosiński, Review and comparison of current experimental approaches for in-situ measurements of building walls thermal transmittance, Energy Build. 203 (2019), https://doi.org/10.1016/j.enbuild.2019.109417.

[12] Standardization, I.O. for ISO 6946:2021-12. Build, Components Build. Elem. – Therm. Resist. Therm. Transm. – Calc. Method, Geneva, Switz, 2021.

[13] C. Peng, Z. Wu, In situ measuring and evaluating the thermal resistance of building construction, Energy Build. 40 (2008) 2076–2082, https://doi.org/10.1016/j.enbuild.2008.05.012.

[14] D. Bienvenido-Huertas, R. Rodríguez-Álvaro, J.J. Moyano, F. Rico, D. Marín, Determining the U-value of fa ades using the thermometric method: potentials and limitations, Energies 11 (2018), https://doi.org/10.3390/en11020360.

[15] H. Krstić, I. Miličević, D. Markulak, M. Domazetović, Thermal Performance Assessment of a Wall Made of Lightweight Concrete Blocks with Recycled Brick and Ground Polystyrene, 2021.

[16] L. Evangelisti, C. Guattari, F. Asdrubali, Influence of heating systems on thermal transmittance evaluations: simulations, experimental measurements and data post-processing, Energy Build. 168 (2018) 180–190, https://doi.org/10.1016/j.enbuild.2018.03.032.

[17] D. Feuermann, Measurement of envelope thermal transmittances in multifamily buildings, Energy Build. 13 (1989) 139–148.

[18] F. Wang, D. Wang, X. Wang, J. Yao, A data analysis method for detecting wall thermal resistance considering wind velocity in situ, Energy Build. 42 (2010) 1647–1653, https://doi.org/10.1016/j.enbuild.2010.04.007.

[19] L. Evangelisti, C. Guattari, F. Asdrubali, Comparison between heat-flow meter and air-surface temperature ratio techniques for assembled panels thermal characterization, Energy Build. 203 (2019), https://doi.org/10.1016/j.enbuild.2019.109441.

[20] G. Desogus, S. Mura, R. Ricciu, Comparing different approaches to in situ measurement of building components thermal resistance, Energy Build. 43 (2011) 2613–2620, https://doi.org/10.1016/j.enbuild.2011.05.025.

[21] B. Mobaraki, S. Komarizadehasl, F.J. Castilla Pascual, J.-A. Lozano-Galant, Application of low-cost sensors for accurate ambient temperature monitoring, Buildings 12 (2022) 1411.

[22] P.G. Cesaratto, M. De Carli, A measuring campaign of thermal conductance in situ and possible impacts on net energy demand in buildings, Energy Build. 59 (2013) 29–36, https://doi.org/10.1016/j.enbuild.2012.08.036.

[23] X. Meng, B. Yan, Y. Gao, J. Wang, W. Zhang, E. Long, Factors affecting the in situ measurement accuracy of the wall heat transfer coefficient using the heat flow meter method, Energy Build. 86 (2015) 754–765, https://doi.org/10.1016/j.enbuild.2014.11.005.

[24] R. Walker, S. Pavía, Thermal performance of a selection of insulation materials suitable for historic buildings, Build. Environ. 94 (2015) 155–165, https://doi.org/10.1016/j.buildenv.2015.07.033.

[25] X. Meng, Y. Gao, Y. Wang, B. Yan, W. Zhang, E. Long, Feasibility experiment on the simple hot box-heat flow meter method and the optimization based on simulation reproduction, Appl. Therm. Eng. 83 (2015) 48–56, https://doi.org/10.1016/j.applthermaleng.2015.03.010.

[26] G. Ficco, F. Iannetta, E. Ianniello, F.R. D'Ambrosio Alfano, M. Dell'Isola, U-value in situ measurement for energy diagnosis of existing buildings, Energy Build. 104 (2015) 108–121, https://doi.org/10.1016/j.enbuild.2015.06.071.

[27] K. Gaspar, M. Casals, M. Gangolells, A comparison of standardized calculation methods for in situ measurements of façades U-value, Energy Build. 130 (2016) 592–599, https://doi.org/10.1016/j.enbuild.2016.08.072.

[28] I.A. Atsonios, I.D. Mandilaras, D.A. Kontogeorgos, M.A. Founti, A comparative assessment of the standardized methods for the in–situ measurement of the thermal resistance of building walls, Energy Build. 154 (2017) 198–206, https://doi.org/10.1016/j.enbuild.2017.08.064.

[29] K. Gaspar, M. Casals, M. Gangolells, In situ measurement of façades with a low U-value: avoiding deviations, Energy Build. 170 (2018) 61–73, https://doi.org/10.1016/j.enbuild.2018.04.012.

[30] L. Evangelisti, C. Guattari, R. De Lieto Vollaro, F. Asdrubali, A methodological approach for heat-flow meter data post-processing under different climatic conditions and wall orientations, Energy Build. 223 (2020), 110216, https://doi.org/10.1016/j.enbuild.2020.110216.

[31] J.M. Andújar Márquez, M.Á. Martínez Bohórquez, S. Gómez Melgar, A new metre for cheap, quick, reliable and simple thermal transmittance (U-value) measurements in buildings, Sensors 17 (2017) 2017, https://doi.org/10.3390/s17092017.

[32] V. Echarri-Iribarren, C. Sotos-Solano, A. Espinosa-Fernández, R. Prado-Govea, The passivhaus standard in the Spanish mediterranean: evaluation of a house's thermal behaviour of enclosures and airtightness, Sustain. Times 11 (2019), https://doi.org/10.3390/su11133732.

[33] D. Bienvenido-Huertas, J. Moyano, C.E. Rodríguez-Jiménez, D. Marín, Applying an artificial neural network to assess thermal transmittance in walls by means of the thermometric method, Appl. Energy 233–234 (2019) 1–14, https://doi.org/10.1016/j.apenergy.2018.10.052.

[34] A. Ahmad, M. Maslehuddin, L.M. Al-Hadhrami, In situ measurement of thermal transmittance and thermal resistance of hollow reinforced precast concrete walls, Energy Build. 84 (2014) 132–141, https://doi.org/10.1016/j.enbuild.2014.07.048.

[35] E. Lucchi, Thermal transmittance of historical stone masonries: a comparison among standard, calculated and measured data, Energy Build. 151 (2017) 393–405, https://doi.org/10.1016/j.enbuild.2017.07.002.

[36] American Society for Testing Material ASTMC 177-97: Standard Test Method For Steady-State Heat Flux Measurements and Thermal Transmission Properties by Means of the Guarded-Hot-Plate Apparatus, Annual Book of ASTM Standards, West Conshohocken, 2000.

[37] P. Achenbakh, Design of a calibrated hot-box for measuring the heat, air, and moisture transfer of composite building walls, in: Thermal Performance of the Exterior Envelopes of Buildings. Proceeding-1, 1981, pp. 308–324.

[38] ASTM (Society for Testing and Materials) Standard Practice for In-Situ Measurement of Heat Flux and Temperature on Building Envelope Components, 2013.

[39] ISO 9869-1:2014 Thermal Insulation - Building Elements - In-Situ Measurement of Thermal Resistance and Thermal Transmittance - Part 1: Heat Flow Meter Method, 2014.

[40] P. Baker, U-values and traditional buildings-in situ measurements and their comparisons to calculated values, Hist. Scotland, Conserv. Gr. 10 (2011) 1–70.

[41] A. Kirimtat, O. Krejcar, A review of infrared thermography for the investigation of building envelopes: advances and prospects, Energy Build. 176 (2018) 390–406, https://doi.org/10.1016/j.enbuild.2018.07.052.
[42] R. Di Maio, E. Piegari, C. Mancini, A. Chiapparino, Quantitative analysis of pulse thermography data for degradation assessment of historical buildings, Eur. Phys. J. Plus 130 (2015), https://doi.org/10.1140/epjp/i2015-15105-6.
[43] E. Lucchi, Thermal transmittance of historical brick masonries: a comparison among standard data, analytical calculation procedures, and in situ heat flow meter measurements, Energy Build. 134 (2017) 171–184, https://doi.org/10.1016/j.enbuild.2016.10.045.
[44] E. Lucchi, F. Roberti, T. Alexandra, Definition of an experimental procedure with the hot box method for the thermal performance evaluation of inhomogeneous walls, Energy Build. 179 (2018) 99–111, https://doi.org/10.1016/j.enbuild.2018.08.049.
[45] M. Andreotti, M. Calzolari, P. Davoli, L.D. Pereira, E. Lucchi, R. Malaguti, Design and construction of a new metering hot box for the in situ hygrothermal measurement in dynamic conditions of historic masonries, Energies 13 (2020), https://doi.org/10.3390/en13112950.
[46] M. Mahmoodzadeh, V. Gretka, K. Hay, C. Steele, P. Mukhopadhyaya, Determining overall heat transfer coefficient (U-value) of wood-framed wall assemblies in Canada using external infrared thermography, Build. Environ. 199 (2021), 107897, https://doi.org/10.1016/j.buildenv.2021.107897.
[47] M. Komary, S. Komarizadehasl, N. Toši, I. Segura, J.A. Lozano-galant, J. Turmo, Low-cost technologies used in corrosion monitoring, Sensors 23 (2023) 1309.
[48] E. Husni, G. Prayoga, J. Tamba, Y. Retnowati, F. Fauzandi, R. Yusuf, B. Yahya, Microclimate investigation of vehicular traffic on the urban heat island through IoT-based device, SSRN Electron. J. 8 (2022), e11739, https://doi.org/10.2139/ssrn.4031262.
[49] B. Brik, M. Esseghir, L. Merghem-Boulahia, H. Snoussi, An IoT-based deep learning approach to analyse indoor thermal comfort of disabled people, Build. Environ. (2021) 203, https://doi.org/10.1016/j.buildenv.2021.108056.
[50] J. Qu, Research on energy saving of computer rooms in Chinese colleges and universities based on IoT and edge computing technology, Heliyon 8 (2022), e10970, https://doi.org/10.1016/j.heliyon.2022.e10970.
[51] A. Luna-Navarro, P. Fidler, A. Law, S. Torres, M. Overend, Building impulse toolkit (BIT): a novel IoT system for capturing the influence of façades on occupant perception and occupant-façade interaction, Build. Environ. 193 (2021), 107656, https://doi.org/10.1016/j.buildenv.2021.107656.
[52] J. Kim, S. Kim, S. Bae, M. Kim, Y. Cho, K.I. Lee, Indoor environment monitoring system tested in a living lab, Build. Environ. 214 (2022), 108879, https://doi.org/10.1016/j.buildenv.2022.108879.
[53] R. Porras Soriano, B. Mobaraki, J.A. Lozano-Galant, S. Sanchez-Cambronero, F. Prieto Muñoz, J.J. Gutierrez, New image recognition technique for intuitive understanding in class of the dynamic response of high-rise buildings, Sustainability 13 (2021) 3695, https://doi.org/10.3390/su13073695.
[54] C. Gameli Hodoli, F. Coulon, M.I. Mead, Applicability of factory calibrated optical particle counters for high-density air quality monitoring networks in Ghana, Heliyon 6 (2020), e04206, https://doi.org/10.1016/j.heliyon.2020.e04206.
[55] B. Mobaraki, S. Komarizadehasl, F. Javier, C. Pascual, J. Antonio, Determination of environmental parameters based on Arduino based low-cost sensors, in: Proceedings of the Recent Trends in Construction and Education RTCEE International Conference, 2020, pp. 10–11.
[56] A.S. Ali, C. Cote, M. Heidarnejad, B. Stephens, Elemental: an open-source wireless hardware and software platform for building energy and indoor environmental monitoring and control, Sensors 19 (2019) 20, https://doi.org/10.3390/s19184017.
[57] V. Echarri, A. Espinosa, C. Rizo, Thermal transmission through existing building enclosures: destructive monitoring in intermediate layers versus non-destructive monitoring with sensors on surfaces, Sensors 17 (2017) 2848, https://doi.org/10.3390/s17122848.
[58] B. Mobaraki, S. Komarizadehasl, F.J. Castilla Pascual, J.A. Lozano-Galant, Open source platforms for monitoring thermal parameters of structures, in: Proceedings of the Bridge Maintenance, Safety, Management, Life-Cycle Sustainability and Innovations, 2019, pp. 3892–3896.
[59] B. Mobaraki, F. Lozano-Galant, R.P. Soriano, F.J.C. Pascual, Application of low-cost sensors for building monitoring: a systematic literature review, Buildings 11 (2021) 336, https://doi.org/10.3390/BUILDINGS11080336.
[60] B. Mobaraki, F.J. Castilla Pascual, F. Lozano-Galant, R. Porras, J.-A. Lozano-Galant, Characterization of the thermal transmittance in buildings using low-cost temperature sensors, 5TH Int. Conf. Build. ENERGY Environ. (2022) 1–8.
[61] Instituto Eduardo Torroja CTE Código Técnico de La Edificación, Catálogo de Elementos Constructivos (CEC), 2010.
[62] S. Kim, J. Seo, H. Jeong, J. Kim, In situ measurement of the heat loss coefficient of thermal bridges in a building envelope, Energy Build. (2022) 256, https://doi.org/10.1016/j.enbuild.2021.111627.
[63] B. Mobaraki, S. Komarizadehasl, F.J. Castilla Pascual, J.A. Lozano-galant, R. Porras Soriano, A novel data acquisition system for obtaining thermal parameters of building envelopes, Buildings 12 (2022) 670, https://doi.org/10.3390/buildings12050670.
[64] B. Mobaraki, F.J. Castilla Pascual, F. Lozano-galant, J.A. Lozano-galant, R. Porras, In situ U-value measurement of building envelopes through continuous low-cost monitoring, Case Stud. Therm. Eng. 43 (2023), 102778, https://doi.org/10.1016/j.csite.2023.102778.
[65] Sensirion SHT35 Available online: https://sensirion.com/products/catalog/SHT35-DIS-F/.
[66] Melexis MLX90614 Available online: https://www.mouser.es/new/melexis/melexis-mlx90640-fir-sensor/.
[67] L. Evangelisti, A. Scorza, R.D.L. Vollaro, S.A. Sciuto, Comparison between heat flow meter (HFM) and thermometric (THM) method for building wall thermal characterization: latest advances and critical review, Sustain. Times 14 (2022) 693, https://doi.org/10.3390/su14020693.